J. Fluid Mech. (1992), *vol.* 236, *pp.* 61–94
Printed in Great Britain

Coupled convective and morphological instability in a simple model of the solidification of a binary alloy, including a shear flow

By S. A. FORTH† AND A. A. WHEELER
School of Mathematics, University Walk, Bristol, BS8 1TW, UK

(Received 14 December 1990)

In this paper we provide a detailed description of the interaction of solutal convection and morphological instability in the presence of a model boundary-layer flow. We present a detailed investigation of the structure of the marginal surfaces in Rayleigh-number, Sekerka-number, Reynolds-number space associated with a linear stability analysis. We give mathematical arguments and physical mechanisms to explain the results and present a coherent description of this complicated situation. We identify two new modes, one convective and one morphological. We show that the oscillatory so-called 'mixed' modes that result from the coupling of morphological and convective modes play a central role in the unfolding of the solution structure by the shear flow. This flow has the effect of decoupling the convective and morphological modes.

1. Introduction

The unidirectional solidification of a binary alloy in a temperature gradient is the main technique by which many electronic materials are produced. These materials are used in the fabrication of electronic devices such as microprocessors, memory chips and infra-red detectors. The rapid development of modern electronic technology over the last thirty years has made ever increasing demands on the quality of these materials, which in turn has stimulated increasing theoretical interest in the mathematical modelling of unidirectional solidification.

In a terrestrial environment the presence of gravity gives rise to convection in the melt. This is recognized to have a profound influence on the dynamics of the freezing solid–liquid interface and hence the quality of the solidified material. In particular, flow in the melt affects the heat and mass transfer within the system and gives rise to spatial and temporal variations in the flow and composition of the melt. This results in a crystal with non-uniform physical properties, such as alloy composition or lattice defect density, which affect the electronic performance of devices made from it.

In the absence of flow in the melt it has long been recognized that a planar solid–liquid interface of a solidifying alloy may experience a transition to a non-planar state. This is known as the morphological instability (Rutter & Chalmers 1953). The physical mechanism by which this occurs can be identified with the variation of the freezing temperature of the molten alloy with its composition, which under certain growth conditions, may result in the formation of a region of melt

† Present address: British Aerospace, Sowerby Research Centre, FPC 266, PO Box 5, Filton, Bristol, UK.

below its freezing temperature adjacent to the interface. In this situation the melt is said to be constitutionally supercooled. The linear stability analysis of this situation was first conducted by Mullins & Sekerka (1964) who theoretically clarified the notion of constitutional supercooling. They only considered stationary modes of instability. It is only recently (Coriell *et al.* 1987) that the exchange of stabilities has been proved for morphological instability under certain conditions upon the thermal field. The first weakly nonlinear investigation of the morphological instability was conducted by Wollkind & Segel (1970) and a numerical investigation of the fully nonlinear regime was first performed by Ungar & Brown (1984), using numerical continuation techniques. For details of more recent developments in this area the reader is referred to the review by Coriell, McFadden & Sekerka (1985).

Convection in the melt can be identified with two different mechanisms: buoyancy induced flow due to gravity or forced flow due to large-scale fluid motion in the melt. Forced flows may arise by, for example, stirring of the melt, which results in the formation of a boundary-layer flow adjacent to the interface. The inclusion of convection substantially complicates the mathematical analysis. For example, it results in a non-autonomous differential operator in the specification of the linear stability problem which in general has no explicit analytic solution. Moreover, it increases the number of non-dimensional control parameters, which when combined with the additional complexity of the solution structure has resulted in difficulty in obtaining a coherent view of this situation.

The convective mode of instability due to buoyancy exists in the absence of a deformable freezing interface. It is generated by unstable density gradients due to the base state, which consists of an exponentially decaying composition into the melt. This problem was first considered by Gershuni & Zhukovitskii (1976) and more recently by Hurle, Jakeman & Wheeler (1983). The convective mode is most unstable at order-one wavenumbers (with respect to the characteristic solute diffusion length) via a stationary mode of instability, with a critical Rayleigh number that depends solely on the segregation coefficient, k.

Coriell *et al.* (1980) were the first to consider the interaction of both buoyancy and morphological modes of instability together. They conducted a linear stability analysis and gave numerical results for a model lead–tin alloy. They found at high enough growth rates that the system is unstable to a morphological mode of instability characterized by a large critical wavenumber. Beneath a certain value of the growth rate the system is unstable to a convective mode with a much lower critical wavenumber, in which solutally induced buoyancy effects predominate. Thermal convection was only found to be significant at very low growth rates. Subsequently, Hurle, Jakeman & Wheeler (1982) and Caroli *et al.* (1985) also considered this situation, but in more detail and in the absence of thermal convection, by employing semi-analytical methods.

It emerges from these works that the morphological mode is very weakly affected by the buoyancy-induced flow because of the short lengthscale associated with the high critical wavenumber of the morphological mode inhibits its influence. However, at order-one wavenumbers a much stronger coupling exists which results in two so-called 'mixed' modes which connect the stationarily stable morphological modes at higher wavenumbers to the stationarily stable convective modes at lower wavenumbers. For the material parameters and growth conditions considered the mixed modes were not found to be the most unstable. Schaeffer & Coriell (1982) repeated these calculations for succinitrile containing ethanol and found that under some growth conditions the mixed modes could be the most unstable. Jenkins (1990)

also found that the mixed modes could be the most unstable, but only when the effect of capillarity is very strong. The weakly nonlinear development of the coupled problem has been addressed by Jenkins (1985*a*, *b*) who found that hexagonal planforms were preferred. Developments in this area are reviewed by Glicksman, Coriell & McFadden (1986).

The effect of a boundary-layer flow on the morphological mode of instability was first considered by Delves (1968, 1971), who considered the imposition of quadratic and Blasius boundary-layer flows adjacent to the interface. More recently Forth & Wheeler (1989) considered the effect of another model boundary-layer flow, namely the asymptotic suction boundary-layer profile. They showed, using both analytical and numerical techniques that the hydrodynamic stability of the boundary layer was largely unaffected by the presence of the freezing interface and that the effect of the flow on the morphological mode of instability was to generate travelling waves. Coriell *et al.* (1984) considered the effect of a plane Couette flow on both the morphological and convective modes for the model lead–tin alloy. They concluded that the effect of the flow was to decouple the two modes. McFadden, Coriell & Alexander (1988) considered the effect of a stagnation-point flow, but limited their analysis to considering only modes perpendicular to the flow.

The coupled problem in the presence of a shear flow has been investigated by Davis and his co-workers (reviewed by Davis 1990) by exploiting different limits of the problem as the segregation coefficient becomes small or the capillarity coefficient large, which permits the derivation of nonlinear amplitude equations for long-wavelength modes.

In this paper we seek to build on the work discussed above to investigate the effect of a boundary-layer flow, modelled by the asymptotic suction boundary-layer profile, on coupled morphological and convective instability. In comparison to previous work we provide a very detailed description of the complicated solution structure of the eigenvalue problem that arises from the linear stability analysis. From this we employ both mathematical and physical arguments to elucidate the interaction between convection in the melt and the freezing interface. Unlike previous workers we present our results in terms of the non-dimensional control parameters: the Rayleigh number, Ra; Reynolds number, Re; and Sekerka number, Sk; in order to describe the marginal surface in (Sk, Ra, Re, γ)-space, where γ is the wavenumber of the disturbance. This allows us to interpret our results as being applicable to a wide range of materials under common growth conditions, other than just the lead–tin alloy specifically considered here. We show that the interaction of buoyancy and the interface gives rise to *two* morphological and *two* convective modes, both of which are stationary, and in addition two mixed modes which are overstable. The introduction of flow breaks a symmetry of the differential operator and results in an unfolding of the solution structure. The mixed modes play a key role in relating the different modes. We are able to provide a coherent physical description of the effect of the boundary-layer flow in order to understand the unfolding. In this description we identify the competition between the unperturbed and perturbed flow as favouring backward and forward travelling waves respectively, which, when combined with the opposite phase differences associated with the convective and morphological modes results in a sympathetic interaction between the backward travelling mixed mode and the morphological modes, and the forward travelling mixed mode and the convective modes in the presence of an imposed boundary-layer flow.

In the next section we briefly describe the model and give the dimensionless

governing equations and steady state associated with the planar interface. In §3 we conduct the linear stability analysis. In §4 we describe the numerical method and in §§5 and 6 give our results. In view of the complexity of the problem and its solution structure we present the results in stages. In §5 we describe the effect of buoyancy alone. We section the marginal surfaces in (Sk, Ra, γ)-space on planes Ra = constant. We display the eigenfunctions associated with the different modes and discuss their identification in terms of the relative phase of the perturbed flow and interface deformation. We show that either convective or morphological modes will be the most unstable depending on the ratio of the Rayleigh number to the Sekerka number and generalize this criterion to alloys for which the capillarity parameter is small and the Schmidt number large. In §6.1 we discuss the effect of a shear flow alone and provide physical arguments for the formation of backward and travelling waves. In §6.2 we describe the effect of flow by sectioning (Sk, Ra, γ)-space on planes Ra = constant, but for a Reynolds number of 5.

2. The model

We consider a dilute binary alloy solidifying vertically upwards due to the presence of an imposed temperature gradient. The solid–liquid interface is initially planar and advances with speed V_0 in a direction opposite to gravity. We shall consider the breakdown of this state to both convective and morphological instability. Further, we suppose that the principal effect of large-scale convection in the melt upon the interface is to produce a momentum boundary-layer flow adjacent to it. We simply model this flow by assuming that it induces a lateral velocity component U_∞ outside the boundary layer. We also assume that because typically the diffusivity of solute (the dilute component of the alloy) is much less than that of both momentum and heat, large-scale transport processes in the melt ensure that the concentration of solute is constant in the bulk of the melt and takes the value C_∞. The system configuration is shown in figure 1. To model this situation we employ a generalization of the one-sided model (Langer 1980) to include fluid motion in the melt. Thus we make the frozen temperature assumption in which the temperature field $T\,(= T^0 + \mathscr{G} z^*)$ is one-dimensional, depending linearly on the vertical coordinate z^*. Here T^0 is the temperature of the planar solid–liquid interface and $\mathscr{G}$ is the temperature gradient. This results from assuming that latent heat effects are negligible, the thermal conductivities of both phases are equal and the thermal diffusive lengthscale is much greater than the solute diffusive lengthscale. We also assume that diffusion of solute in the solid phase is negligible. The melt is modelled by an incompressible Newtonian Boussinesq fluid in which the density depends solely upon the solute concentration.

We take a coordinate system moving at speed V_0 coincident with the average position of the initially planar interface. Further, we non-dimensionalize the system with respect to the characteristic scales of the solute field by defining

$$\boldsymbol{x}^* = \frac{D}{V_0}\boldsymbol{x}, \quad t^* = \frac{D}{V_0^2}t, \quad h^* = \frac{D}{V_0}h, \quad \boldsymbol{u}^* = V_0\boldsymbol{u}, \quad C^* = C_\infty C, \quad p^* = \frac{\nu\rho V_0^2}{\tilde{D}}p,$$

where a superscript asterisk represents a dimensional quantity, $\boldsymbol{x}$ is the position vector, t is time, $\boldsymbol{u}$ is the velocity in the melt and C is the solute concentration in the melt, p is the pressure and $z = h(x, y, t)$ is the interface position. Here ρ and $\tilde{D}$ are the

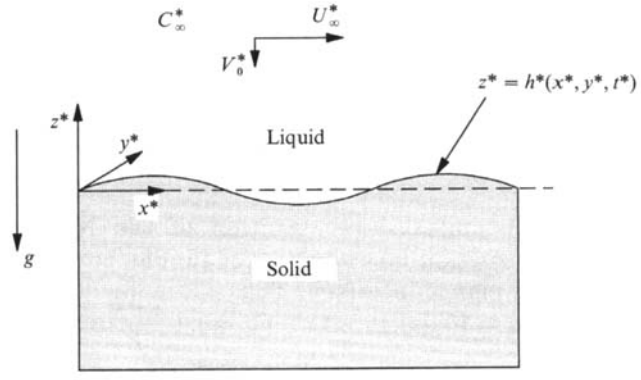

FIGURE 1. Configuration diagram.

density of the melt and the diffusivity of the solute in the melt. The governing equations are then

$$Sc^{-1}\left\{\frac{\partial \boldsymbol{u}}{\partial t}+\boldsymbol{u}\cdot\nabla\boldsymbol{u}\right\} = -\nabla p+\nabla^2\boldsymbol{u}-Ra\frac{k}{1-k}C\boldsymbol{k},$$

$$\frac{\partial C}{\partial t}+\boldsymbol{u}\cdot\nabla C = \nabla^2 C,$$

$$\nabla\cdot\boldsymbol{u} = 0.$$

We assume that there is no density change on solidification and hence conservation of mass across the interface gives that

$$(\boldsymbol{u}+\boldsymbol{k})\cdot\boldsymbol{n} = 0, \quad z = h(x,y,t),$$

the no-slip condition at the interface gives that

$$(\boldsymbol{u}+\boldsymbol{k})\times\boldsymbol{n} = 0, \quad z = h(x,y,t),$$

conservation of solute there implies that

$$\frac{\partial C}{\partial \boldsymbol{n}} = (k-1)(1+h_t)\,\boldsymbol{k}\cdot\boldsymbol{n}C, \quad z = h(x,y,t),$$

and the assumption of local thermodynamic equilibrium there gives

$$Sk^{-1}h = \frac{k}{k-1}\left(C-\frac{1}{k}\right)+U\mathscr{K}, \quad z = h(x,y,t).$$

Further, far from the interface we have that

$$C\to 1, \quad \boldsymbol{u}\to Re\,\boldsymbol{i}-\boldsymbol{k} \quad \text{as} \quad z\to\infty.$$

Here $\boldsymbol{i},\boldsymbol{k},\boldsymbol{n}$ are the unit vectors in the x,z directions and the unit normal to the interface $z = h(x,y,t)$ respectively and $\mathscr{K}$ is the curvature of the interface, which is taken to be negative for projections into the melt. The dimensionless groups controlling the system are

$$Ra = \frac{C_\infty \tilde{D}^2 g\tilde{\alpha}(1-k)}{\nu k V_0^3}, \quad Sk = \frac{mC_\infty(k-1)V_0}{k\tilde{D}\mathscr{G}}, \quad \mathscr{U} = \frac{T^*\Gamma V_0 k}{mC_\infty\tilde{D}(k-1)}, \quad Re = \frac{U_\infty}{V_0},$$

$$Sc = \frac{\nu}{\tilde{D}}, k,$$

where Ra is the Rayleigh number, Sk the Sekerka number, $\mathscr{U}$ the dimensionless capillarity parameter, Re the Reynolds number, Sc the Schmidt number and k the segregation coefficient. Here g is the acceleration due to gravity, $\tilde{\alpha}$ the coefficient of volume expansion, ν the kinematic viscosity, m the slope of the liquidus curve, Γ the dimensional capillarity coefficient and T^* the freezing temperature of the pure alloy.

2.1. *Steady state*

We exploit an exact boundary-layer solution of the Navier–Stokes equations, namely the asymptotic suction boundary-layer profile, to provide the steady-state flow corresponding to a planar interface. Thus

$$\boldsymbol{u}_0 = (U_0(z), 0, -1), \quad C_0 = 1 + \frac{1-k}{k}\mathrm{e}^{-z},$$

where $U_0 = Re[1-\exp(-z/Sc)]$, in which the diffusion of both solute and vorticity away from the interface are balanced by advection towards the interface, due to its advance into the melt.

3. Linear stability analysis

We now conduct a linear stability analysis of the above steady state and put

$$\boldsymbol{u} = \boldsymbol{u}_0 + \boldsymbol{u}_1(z)\exp[\mathrm{i}(\alpha(x-ct)+\beta y)],$$
$$C = C_0 + C_1(z)\exp[\mathrm{i}(\alpha(x-ct)+\beta y)],$$
$$h = H_1\exp[\mathrm{i}(\alpha(x-ct)+\beta y)],$$

where α and β are the wavenumbers in thc x- and y-directions and $c = c_\mathrm{r} + \mathrm{i}c_\mathrm{i}$ is the complex wave speed, c_r is the wave speed in the x-direction and αc_i is the linear growth rate. These forms, when inserted into the linearized governing equations and boundary conditions give the following eigenvalue problem for the complex wave speed c, and $C_1(z)$ and $W_1(z)$, the perturbed solute and perturbed axial component of the velocity:

$$\{[\mathrm{D}^2 + \mathrm{Sc}^{-1}(\mathrm{D} - \mathrm{i}\alpha(U_0 - c)) - \gamma^2][\mathrm{D}^2 - \gamma^2] + \mathrm{i}\alpha U_0'' Sc^{-1}\} W_1 = -\gamma^2 Ra \frac{k}{1-k} C_1, \quad z \geqslant 0, \tag{1}$$

$$[\mathrm{D}^2 + \mathrm{D} - \gamma^2 - \mathrm{i}\alpha(U_0 - c)]\, C_1 = -\frac{k-1}{k} W_1 \exp(-z), \quad z \geqslant 0, \tag{2}$$

with

$$W_1 = 0, \quad z = 0, \tag{3}$$

$$\mathrm{D}W_1 - \frac{\mathrm{i}\alpha Re\, k}{Sc(k-1)\,(Sk^{-1} - 1 + \mathscr{U}\gamma^2)} C_1 = 0, \quad z = 0, \tag{4}$$

$$\left[\mathrm{D} + \frac{(1-k)\,(Sk^{-1} + \mathscr{U}\gamma^2) + \mathrm{i}\alpha c - 1}{Sk^{-1} - 1 + \mathscr{U}\gamma^2}\right] C_1 = 0, \quad z = 0, \tag{5}$$

and

$$\mathrm{D}w_1, \mathrm{D}^2 w_1, C_1 \to 0 \quad \text{as} \quad z \to \infty, \tag{6}$$

where $\mathrm{D} \equiv \mathrm{d}/\mathrm{d}z$, and $\gamma = (\alpha^2 + \beta^2)^{\frac{1}{2}}$ is the wavenumber of the disturbance. The interface deflection is given by

$$H_1(Sk^{-1} - 1 + \mathscr{U}\gamma^2) = \frac{k}{k-1} C_1(0). \tag{7}$$

The above eigenvalue problem (1)–(6) is specified by three control parameters: Ra, Re, Sk; and three dimensionless material parameters: k, Sc, and $\mathscr{U}$, which we regard as fixed for a given alloy and growth conditions. Our aim is to determine the relation $f(\alpha, \beta, c_\mathrm{r}, c_\mathrm{i}, Ra, Re, Sk) = 0$, defined by the above eigenvalue problem. In

particular we are interested in the marginal states given by $\alpha c_i = 0$, i.e. $f(\alpha, \beta, c_r, 0, Ra, Re, Sk) = 0$. We now make some remarks regarding this eigenvalue problem.

If the wavenumber in the direction of the flow, α, is zero (though the complex wave speed $-i\alpha c$ is not necessarily zero), then the forced flow plays no role in the determination of the eigensolution and is thus equivalent to setting the Reynolds number to zero. This result was first noted by Delves (1968) and more recently by Coriell *et al.* (1984). This is because if $\alpha = 0$ then the wave vector of the disturbance is normal to the direction of the boundary-layer flow, in which case the forced flow does not contribute to the lateral transport of the perturbed solute and momentum.

We also note that if $\boldsymbol{v} = (W_1(z), C_1(z), H_1, Ra, Re, \alpha, \gamma, c)^T$ is one eigensolution of (1)–(6) then so is $\boldsymbol{v}' = (W_1^*(z), C_1^*(z), H_1^*, Ra, -Re, \alpha, \gamma, -c^*)^T$, where an asterisk denotes complex conjugate. Thus, changing the sign of the Reynolds number does not affect the stability of the system since the growth rate is still αc_i, but the wave speed is now $-c_r$, the same wave travelling in the opposite direction. This simply corresponds to the fact that the imposed flow breaks the left–right symmetry of the system about the plane $x = 0$.

We confine our attention to systems in which the segregation coefficient is less than unity, and we observe from (7) that the sign of $(Sk^{-1} - 1 + \mathscr{U}\gamma^2)$ determines whether the interface and perturbed interfacial solute concentration have the same or opposite phase. Situations in which $(Sk^{-1} - 1 + \mathscr{U}\gamma^2) < 0$ we shall refer to in this paper as constitutionally supercooled, in which case they are in phase; otherwise the system is not supercooled and they are in antiphase. This definition of constitutional supercooling incorporates a capillarity term $(U\gamma^2)$, this differs from the standard one which requires that $Sk^{-1} - 1 < 0$, due to Rutter & Chambers (1953).

4. Numerical procedure

In general the eigenvalue problem (1)–(6) does not admit an analytical non-trivial solution and so we resort to a numerical investigation, in which case there are two non-trivial matters that need to be addressed. The first concerns the application of the far-field boundary conditions (6) which have to be imposed at a finite value of z, z_{end}, say, and the second, the question of how to pose a normalization condition to ensure a non-trivial solution.

Previous authors (for example Coriell *et al.* 1980, 1984) imposed the far-field boundary conditions (6) at $z = z_{end}$ directly. They found that, provided z_{end} was sufficiently large, their solutions were independent of z_{end} and the exact form of the boundary conditions they used. In order to achieve computational efficiency by making z_{end} as small as possible we have adopted 'constant tail conditions' by extending the results reviewed by Ng & Reid (1980) for dealing with the hydrodynamic stability of the asymptotic boundary-layer profile, to include the solute field. The details of this analysis are given by Forth (1989) and result in the following boundary conditions to be applied at $z = z_{end}$:

$$[\mathrm{D} + \tfrac{1}{2} + R_c] C_1 = 0, \tag{8}$$

$$\left[\mathrm{D}^2 + \left(\gamma + R_f + \frac{1}{2Sc}\right)\mathrm{D} + \gamma\left(R_f + \frac{1}{2Sc}\right)\right] W_1 = 0, \tag{9}$$

$$\left[\mathrm{D}^3 - \left[\left(R_f + \frac{1}{2Sc}\right)^2 + \gamma\left(R_f + \frac{1}{2Sc}\right) + \gamma^2\right]\mathrm{D} - \gamma\left(R_f + \frac{1}{2Sc}\right)\left(\gamma + R_f + \frac{1}{2Sc}\right)\right] W_1 = 0, \tag{10}$$

where $R_f = +[\frac{1}{4}Sc^{-2} + \gamma^2 + i\alpha Sc^{-1}(Re - c)]^{\frac{1}{2}}$ and $R_c = +[\frac{1}{4} + \gamma^2 + i\alpha(Re - c)]^{\frac{1}{2}}$.

The second problem, arising from the nature of the eigenvalue problem, is that we need to specify an additional inhomogeneous boundary condition by which to normalize the eigensolution (Keller 1976). We take $C_1(0) = 1$, since for morphological and convective instabilities we anticipate there to be a non-zero perturbation to the solute field. This additional boundary condition overdetermines the system. We thus fixed the control parameters and solved the governing equations (1) and (2) subject to the boundary conditions (3), (4), (8), (9), (10). The residual error in the remaining boundary condition (5) was then determined and the wave speed c iterated until this boundary condition was satisfied to a given numerical precision. The numerical integration was performed using SUPORT (Scott & Watts 1975), a two-point boundary-value problem solver for linear systems of ordinary differential equations. The NAG nonlinear solver C05NBF was employed to update the value of c. All the calculations presented here refer to the model lead–tin alloy considered by Coriell *et al.* (1980) which corresponds to $\mathscr{U} = 6.131 \times 10^{-4}$, $Sc = 81$, and $k = 0.3$. In presenting our results we first consider the system in the absence of a shear flow, $Re = 0$.

5. The effect of buoyancy alone: $Re = 0$

In the absence of a flow there is no preferred direction and without loss of generality we may set the wavenumber in the y-direction, β, to zero, in which case $\alpha \equiv \gamma$. We determine the marginal surfaces in (α, Ra, Sk)-space. In order to elucidate these surfaces we section this space by planes of constant Rayleigh number, varying between 0 and 21. These are shown in figures 2–7. Each figure consists of two diagrams, the upper shows the marginal curves in (α, Sk)-space and the lower the corresponding (α, c_r)-space along the marginal curves. In the upper diagram shaded areas represent unstable regions of parameter space in which there is at least one positive value of the growth rate αc_i. Below we describe the effect of successively increasing the Rayleigh number from zero and hence the effect of increasing buoyancy forces on the system.

5.1. *The morphological mode: $Ra = 0$ and $Re = 0$*

In figure 2 we show the situation corresponding to $Ra = 0$ in which there is no flow. Thus the system is only rendered unstable via a morphological mode of instability. The marginal curve for morphological instability and the corresponding eigenmode are denoted M1. The wave speed along this marginal curve is zero, in agreement with the principal of the exchange of stability which can be proved in this case (Coriell *et al.* 1987). For negative Sekerka number the system is unstable except for the region at high wavenumber where capillarity stabilizes the system. Further, the line $Sk = 0$ also denotes a stability boundary at which the linear growth rate is discontinuous, $\alpha c_i \to -\infty$ as $Sk \to 0^+$ and $\alpha c_i \to +\infty$ as $Sk \to 0^-$. This is because a small positive Sekerka number corresponds to a strongly stabilizing large positive temperature gradient, whereas a small negative Sekerka number corresponds to a highly destabilizing large negative temperature gradient. Thus we consider the plane $Sk = 0$ as a branch cut as regards the morphological mode of instability. It is for this reason that $Sk < 0$ is an unphysical region of this parameter space corresponding to a completely undercooled melt. We denote the stability boundary $Sk = 0$ and the branch of the morphological mode at high wavenumber which lies in the region $Sk < 0$ by UM, as indicated in figure 2.

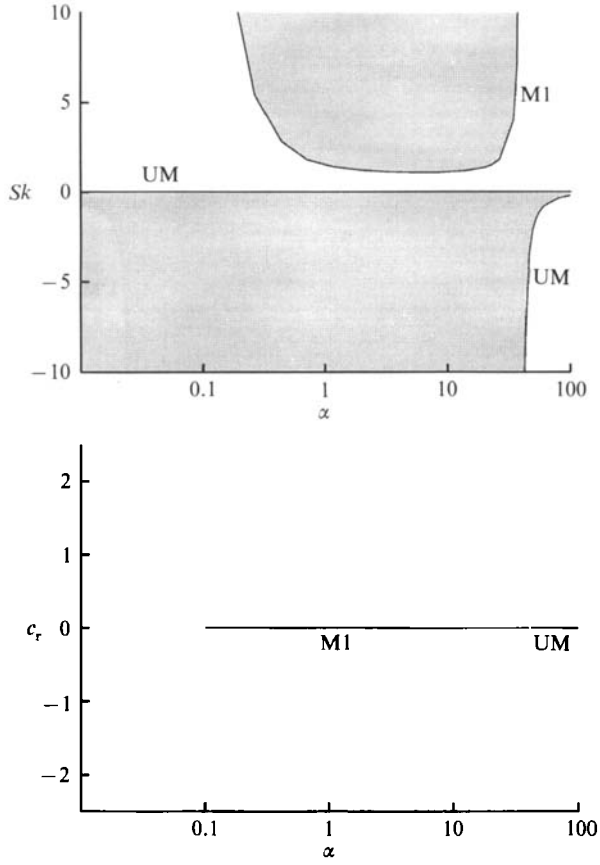

FIGURE 2. The dependence of the Sekerka number, Sk, and wave speed, c, on the wave number, α, of a marginally stable disturbance for the case $Ra = 0$ and $Re = 0$. Shaded areas represent regions in (α, Sk)-space in which the system is unstable. The solid curves labelled M1 and UM represent the marginal states of the different branches of the purely morphological mode.

5.2. *The interaction of convective and morphological modes: $Ra \neq 0$ and $Re = 0$*

From figure 3 we observe that on increasing the Rayleigh number to 7 another distinct unstable region is present. It exists at negative values of the Sekerka number and its marginal curve is indicated by a broken line; we denote it C1. The maximum critical Sekerka number for this mode occurs at a wavenumber of approximately 0.27. Further, its wave speed is also zero and so it is stationarily stable. Below we identify this as a convective mode of instability.

The minimum of the marginal curve corresponding to the morphological mode of instability, M1, is very slightly affected; a weak stabilization being detected. At low wavenumbers the morphological branch has been displaced by two coincident marginal curves corresponding to overstable modes of instability, denoted X1 and X2, which we refer to as mixed modes. These two branches are indicated in figure 3 by a dotted line and correspond to a pair of real eigenvalues for the complex growth rate, $+c_r$ and $-c_r$ respectively, corresponding to a pair of travelling waves. We denote the portion of the marginal curve M1 displaced by the mixed modes as C2, which is indicated in figure 3 by a dashed line. Below we show that the eigenmode associated with the C2 curve is convective in nature.

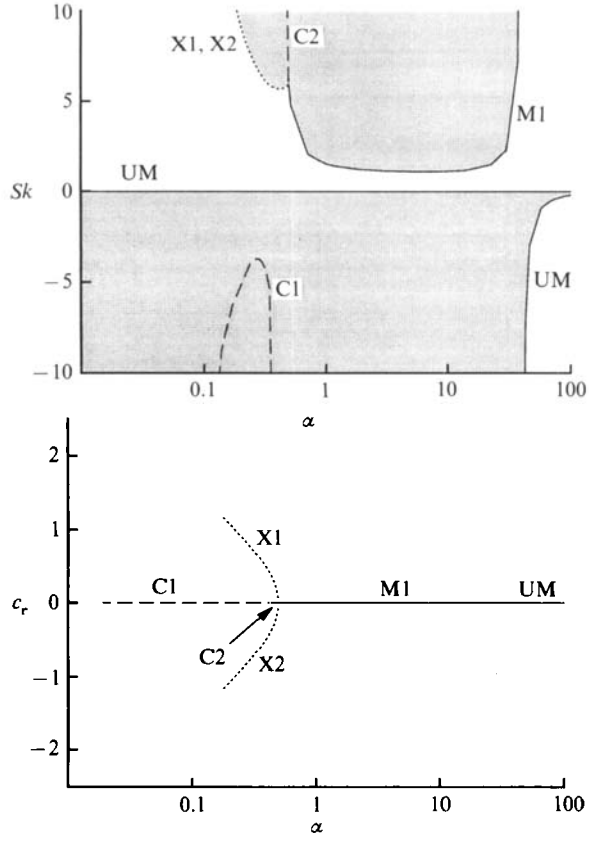

FIGURE 3. As figure 2 but for $Ra = 7$ and $Re = 0$. The dashed curve labelled C1 represents a convective mode and the dotted curves labelled X1 and X2 represent the two overstable mixed modes.

At this Rayleigh number of 7 and a wavenumber about 0.27 the system is morphologically unstable to the mixed modes X1 and X2 for a sufficiently large value of the Sekerka number. As Sk is diminished the system is stabilized at a positive Sekerka number, which on passing through zero renders the system morphologically unstable via the mode UM. Further reduction of the Sekerka number renders the system also unstable to the convective mode C1.

In figure 4 we show the situation for $Ra = 11$. The convective branch C1 has been further destabilized and the system is now convectively unstable at small positive Sekerka numbers over a small range of low wavenumbers. The other significant change is that the mixed modes are also destabilized as they extend to lower values of the Sekerka number. Stability diagrams for Rayleigh numbers of 15, 19 and 21 are shown in figures 5, 6 and 7. As the Rayleigh number increases the mixed modes X1, X2 and the convective mode C1 approach one another and have by $Ra = 21$ joined, resulting in a new stationary mode. We denote the mode along this connection by M2. The result of this connection is that the marginal curves X1 and X2 are separated into distinct portions. The influence of the convective branch on the mixed modes is manifested by the wave speed along the latters' marginal curves, which is reduced as the two modes approach one another. This results in a 'neck' forming in the wave speed curve at $Ra = 19$ where the wave speeds of the forward and backward

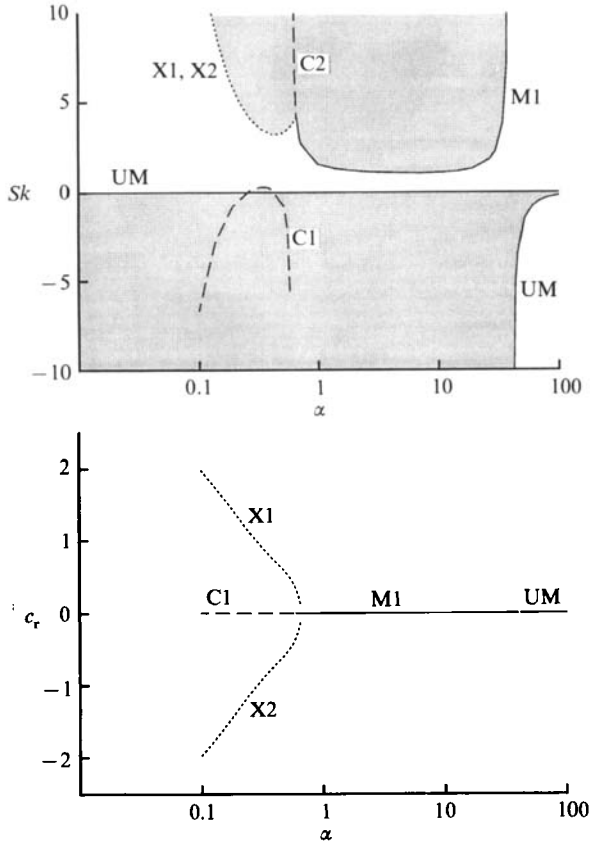

FIGURE 4. As figure 3 but for $Ra = 11$ and $Re = 0$.

travelling waves, X1 and X2, both approach zero. At $Ra = 21$ this effect is increased to give a range of wavenumbers where the wave speed is zero, corresponding to the M2 mode, as well as an isolated loop at higher wavenumbers corresponding to the portion of the X1 and X2 marginal curves connecting the M2 marginal curve with the M1 and C2 marginal curves.

5.2.1. *Detailed study of the case* $Ra = 15$, $Re = 0$

We now investigate the interaction between the different modes in more detail by concentrating on the case $Ra = 15$. In figure 8 we plot the eigenfunctions over one wavelength in the x-direction for five different points on the marginal curves given in figure 5: the minimum of the morphological curve M1, the minima of the mixed-mode branches X1 and X2, the maxima of the convective branch C1 and a point on the branch C2. For each case the eigenfunction has been normalized so that the concentration in the bottom left corner is unity and we display the perturbed stream function (top diagram of each pair), the perturbed concentration (the bottom diagram of each pair) and the interface deflection which is represented above each pair of diagrams together with its amplitude. If the wave speed is non-zero (as is the case for the mixed modes X1, X2) then the frame of reference of each plot is coincident with the travelling wave.

We observe that for the convective mode C1 the fluid rises above the troughs in

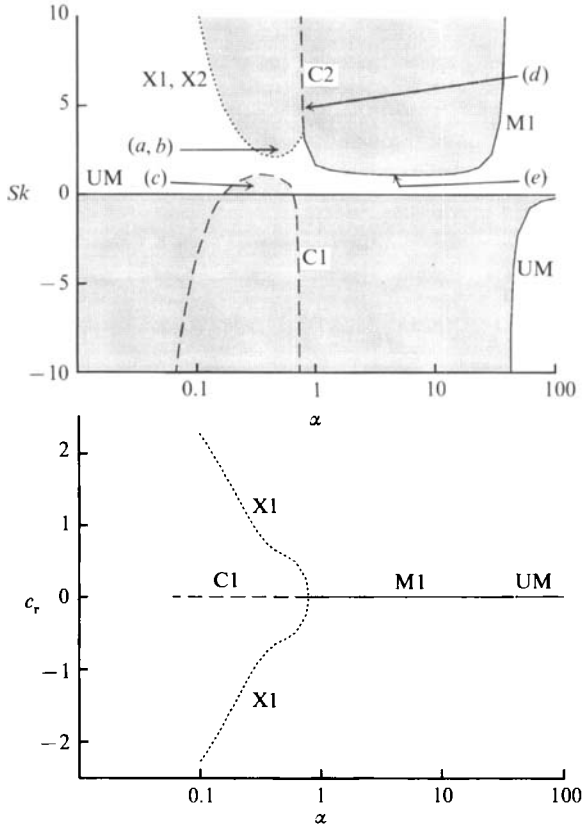

FIGURE 5. As figure 3 but for $Ra = 15$ and $Re = 0$.

the interface and descends at its peaks. This is in contrast to the morphological mode M1 for which the fluid rises above the peaks and descends above the troughs. The maxima of the stream functions for the C1 and M1 modes are approximately 18 and 0.001 respectively, indicating that the convective mode is characterized by a strong flow above an almost planar interface compared to the morphological mode M1, which is characterized by a deformed interface with a weak baroclinic flow in the melt. In the case of the C2 mode the situation is similar to that of the morphological mode M1 but with a much stronger convective flow.

The two mechanisms of morphological and convective instability are in opposition in the sense that they induce upflow and downflow above the peaks, respectively. If the buoyancy forces are sufficiently strong then upflow from trough to peak associated with the morphological mode may be sufficiently buoyant to detach before the peak is attained and similarly the slumping flow from peak to trough associated with the convective mode of instability may rise vertically before reaching the trough. In either of these cases the buoyant plume would be shifted laterally and would cause a phase difference between the solute field and the interface deflection. Such a loss of symmetry would result in preferential freezing on one side of the peaks resulting in a travelling wave, the mixed mode. Davis (1990) observed that the opposite character of the convective and morphological modes given above may be responsible for overstability.

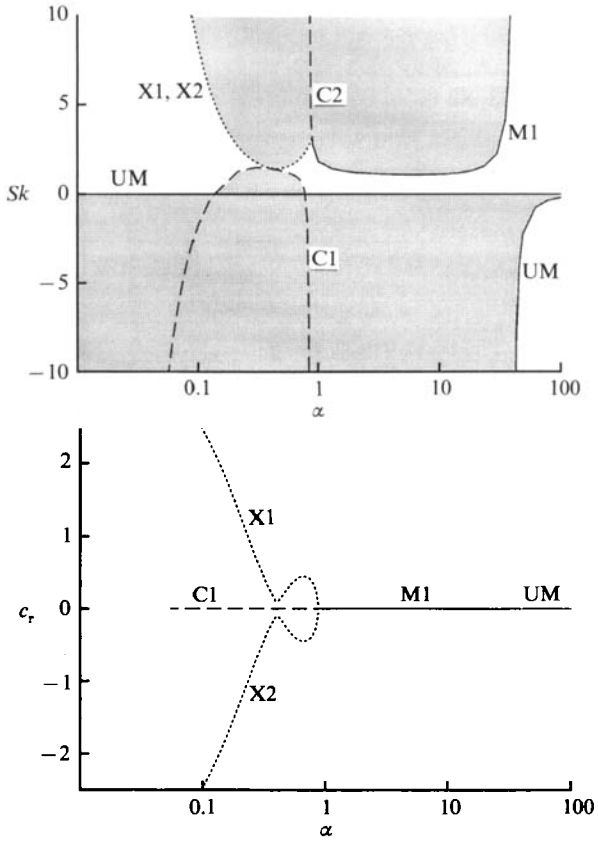

FIGURE 6. As figure 3 but for $Ra = 19$ and $Re = 0$.

5.2.2. *Physical mechanisms*

To gain further insight into the mechanisms by which the various modes are affected by increasing the Rayleigh number we have plotted the real and imaginary parts of the complex wave speed as a function of the Sekerka number for several different values of the wavenumber, for a fixed Rayleigh number of 15. These are given in figures 9 and 10, where the imaginary and real parts of c are given by solid and broken lines respectively. In figure 9 we plot these quantities for $\alpha = 0.5$. At negative Sekerka numbers there is a branch for which the linear growth rate αc_i becomes large as $Sk \to 0^-$ and which we therefore identify as the morphological mode UM. Beneath lies a stationary mode which is stabilized as Sk increases and is identified as the C1 mode. Below this lies another stationary mode, M2, which, in contrast, is destabilized as Sk increases and connects with the C1 mode at a value of Sk slightly greater than unity, whereupon the growth rates of the two modes are equal. Emanating from this limit point are the two mixed modes, X1, X2, whose wave speeds, c_r increase monotonically with Sk. They were found to persist up to $Sk = 20$, the upper limit of our calculations. It is clear from the behaviour of the M2 mode as $Sk \to 0^+$ that it is the continuation of the UM mode to positive values of the Sekerka number.

The situation for a wavenumber of 0.75 is shown in figure 10. As previously, the mode UM exists at negative values of Sk but is not shown. The structure at low wavenumbers is similar to the previous case. However, the two mixed modes are

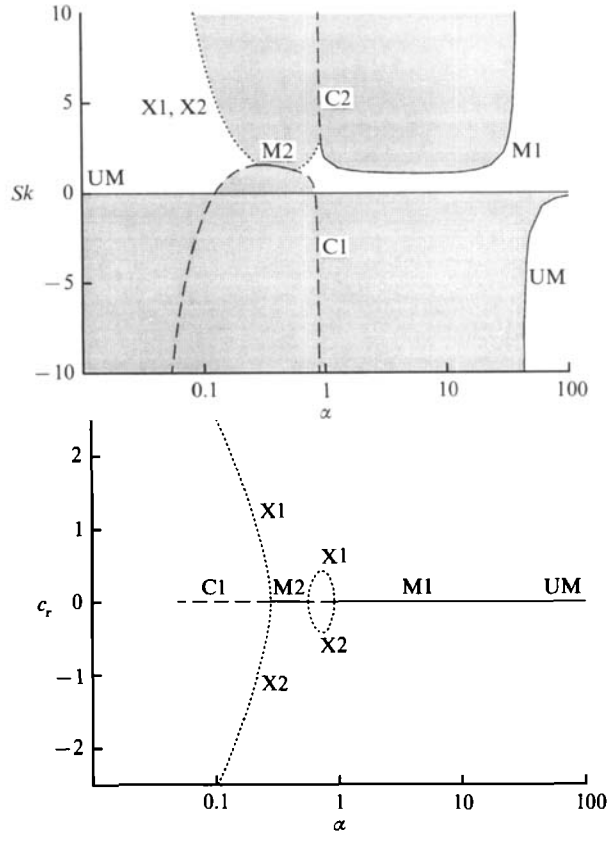

FIGURE 7. As figure 3 but for $Ra = 21$ and $Re = 0$.

found to be now of finite extent and coalesce at the junction of two additional stationary modes. The upper one is destabilized and the lower stabilized by increasing the Sekerka number. Comparison with figure 5 identifies the lower mode as C2 and, below, we find that the upper is the mode M1. It is now evident that the marginal curve corresponding to C2, given in figure 5 represents the C2 mode becoming *stable* as Sk increases and not the morphological mode M1 becoming unstable. In addition we note that the mode M1 is always unstable for this wavenumber and exists only for $Sk > Sk_{M1}$, where Sk_{M1} represents the value of Sk at the limit point of M1 and C2 as indicated in figure 10. Thus we should modify the stability diagram to include this region of instability to the mode M1 which is not bounded by a marginal stability curve; this is shown schematically in figure 11 by a hatched region. In this region the system is unstable to *both* the modes M1 and C2, whereas above the upper boundary of it, given by the chained curve of the C2 mode, it is only unstable to the M1 mode and below the lower boundary of this region, given by a dashed curve, neither the M1 or C2 modes exist.

5.2.3. *The effect of buoyancy on the morphological mode*

We now discuss the effect of buoyancy on the morphological mode M1. We assume that $k < 1$ and than the solute is lighter that the solvent with gravity acting vertically downwards, although the discussion holds *mutatis mutandis* for $k > 1$ and heavy solute. In the absence of buoyancy solute diffusion acts to reduce the

concentration differences along the interface and thus the perturbed solute is maximum at the peaks and minimum at the troughs. Hence when buoyancy effects are included this lateral concentration gradient results in light, solute-rich fluid above the peaks and hence upflow there, with a corresponding downflow above the troughs. Thus an effect of buoyancy is to transport more solute to the peaks from the troughs. This is a stabilizing process as an enhanced solute concentration at the peaks reduces the local freezing temperature which mitigates against any further freezing and hence growth of the peak. It is instructive to conduct an analysis of the eigenvalue problem (1)–(6) in the double limit $Sc \to \infty$, $Ra \to 0$ which gives, after some straightforward analysis, that the perturbed axial velocity is

$$W_1(z) = Ra\, H_1 \frac{k}{(\mu_1^2-\alpha^2)^2(\mu_1+1-k)}[\alpha(\alpha+\mu_1)-a\mu_1 \mathrm{e}^{-az}-\alpha^2 \mathrm{e}^{-\mu_1 z}]+O(Ra^2)+O(Sc^{-1}), \tag{11}$$

where $\mu_1 = \frac{1}{2}[1+(1+4\alpha^2)^{\frac{1}{2}}]$. It is easily shown that, for all $0 < k < 1$, $W_1(z)$ increases monotonically with z and

$$W_1 \to \frac{\alpha k(\alpha+\mu_1)}{(\mu_1+1-k)(\mu_1^2-\alpha^2)^2}+O(Ra^2)+O(Sc^{-1}) \quad (>0) \quad \text{as} \quad z \to \infty. \tag{12}$$

Thus the effect of a *weak* buoyancy force on the morphological mode of instability confirms the above physical argument that it will induce an upflow above the peaks of the interface. This analysis also implies that we cannot impose the condition that the perturbed axial velocity is zero in the bulk of the melt when buoyancy effects are included (although the mean axial velocity over one lateral period of the eigenfunction is zero). A similar result was obtained by Riley & Davis (1990) in a different asymptotic limit of this problem.

5.2.4. *The effect of the interface on the convective mode*

Consider the convective mode of instability C1. In the absence of interface deformation this results in a perturbed concentration with maxima below the less dense rising plumes of fluid. If the Sekerka number is sufficiently small then the system will not be supercooled and hence, as noted at the end of §3, the interface deformation and the perturbed solute will be in antiphase. Thus troughs will form beneath the upflow plumes. This is confirmed by the (stable) C1 mode shown in figure 10(*c*) which corresponds to $Sk = 0.8$ and is therefore not supercooled. If however the melt is supercooled then it appears from the neutral C1 mode shown in figure 8, for which $Sk = 1.109$, that the system accommodates the requirement that the interfacial deformation and perturbed solute concentration be in phase by the formation of a concentration boundary layer adjacent to the interface. It is not clear why the system reacts in this way, rather than allow upflow above the peaks and therefore alleviate the need for such a solute boundary layer. Hence the effect of a freezing interface on the convective mode of instability is a downflow above the peaks and an upflow above the troughs as conjectured by Davis (1990) for the case of a weakly deformable interface. Our results given in figures 2 to 7 indicate that increasing the Sekerka number increases the Rayleigh number for the onset of the convective mode C1 and therefore has a stabilizing effect on the convective mode of instability; however, we are unable to provide a physical mechanism for this.

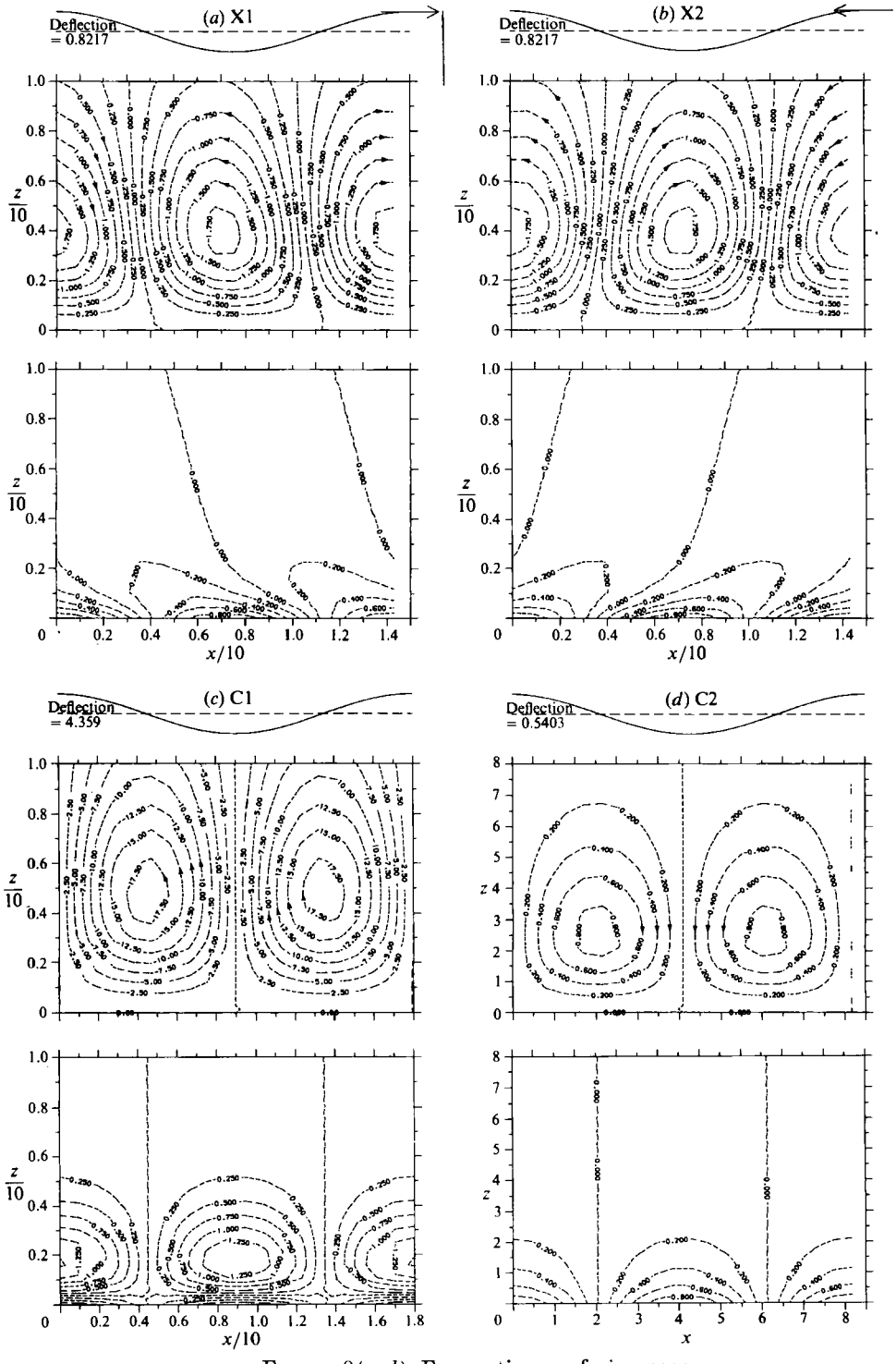

FIGURE 8(*a–d*). For caption see facing page.

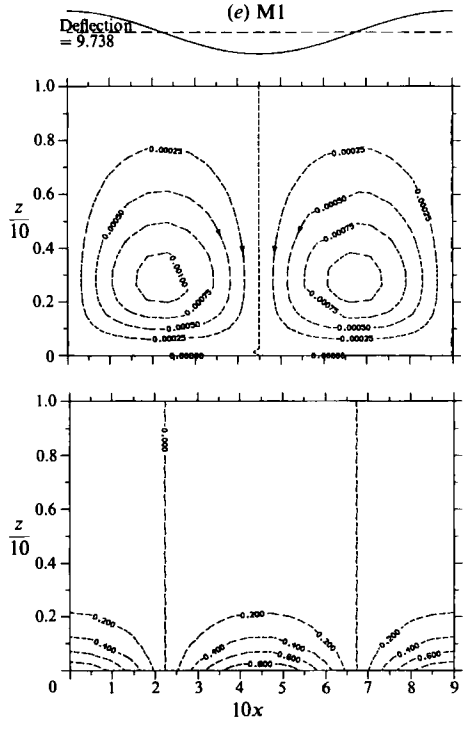

FIGURE 8. The eigenfunctions representative of the different modes for the case $Ra = 15$ and $Re = 0$. Each figure displays the eigenfunctions at the marginal states indicated by the points marked (*a–e*) in figure 5 and shows the perturbed stream function (above) and the perturbed solute concentration (below). We have normalized each eigensolution so that the perturbed concentration at (0, 0) is unity. Above each pair of contour plots is indicated the perturbed interface deflection, its phase but not its amplitude is correctly given. The maximum contour values of the perturbed stream function and solute concentration are respectively: X1, X2, 1.75, 1; C1, 17.5, 1.5; C2, 0.8, 1; M1, 0.001, 1.

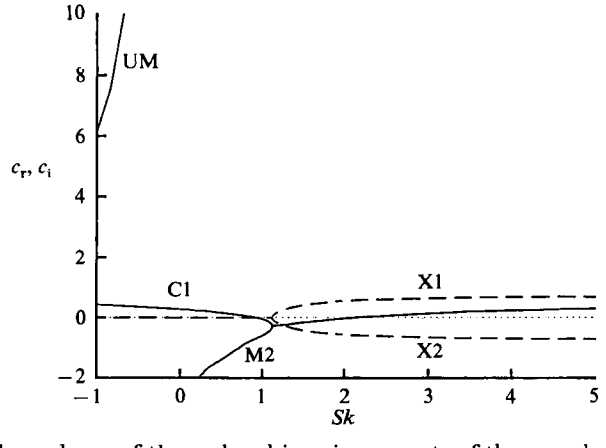

FIGURE 9. The dependence of the real and imaginary parts of the complex wave speed, $c = c_r + ic_i$ for a wavenumber α of 0.5 and a Rayleigh number of 15. The dashed and solid curves represent the real and imaginary parts respectively. The quantity αc_i is the growth rate of the disturbance.

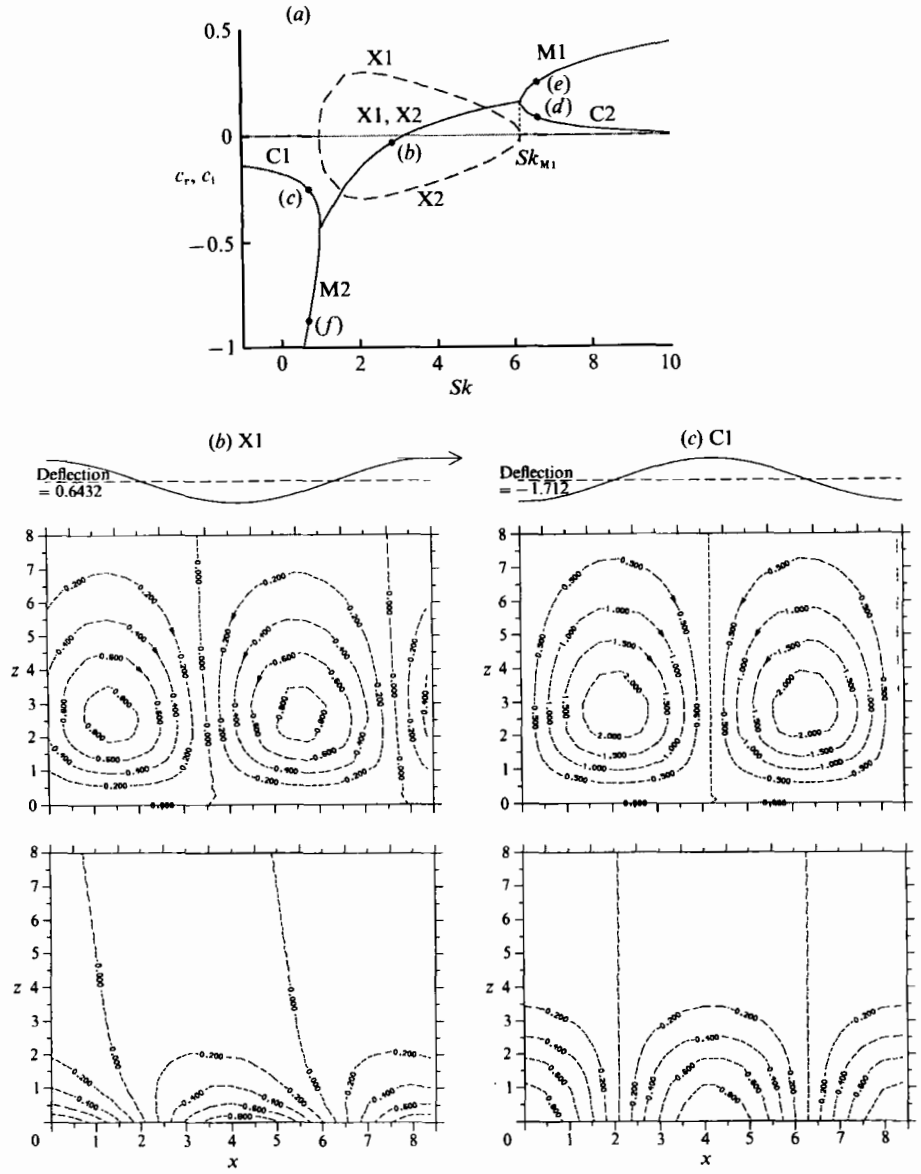

FIGURE 10(*a–c*). For caption see facing page.

5.2.5. *Mathematical characterization of the modes*

Above, we have identified the different eigenfunctions as convective or morphological, based on physical arguments. We now attempt to justify this description from a more mathematical standpoint based on arguments given previously by Caroli *et al.* (1985) and McFadden *et al.* (1988). Our starting point is to describe them individually in isolation as pure modes. Thus in the absence of convection the linear growth rate of the morphological mode would only depend on Sk and similarly that of the convective mode (in the absence of a freezing interface) only on Ra. Therefore their dispersion relations may be written as

$$F_m(\alpha, Sk) + i\alpha c = 0,$$

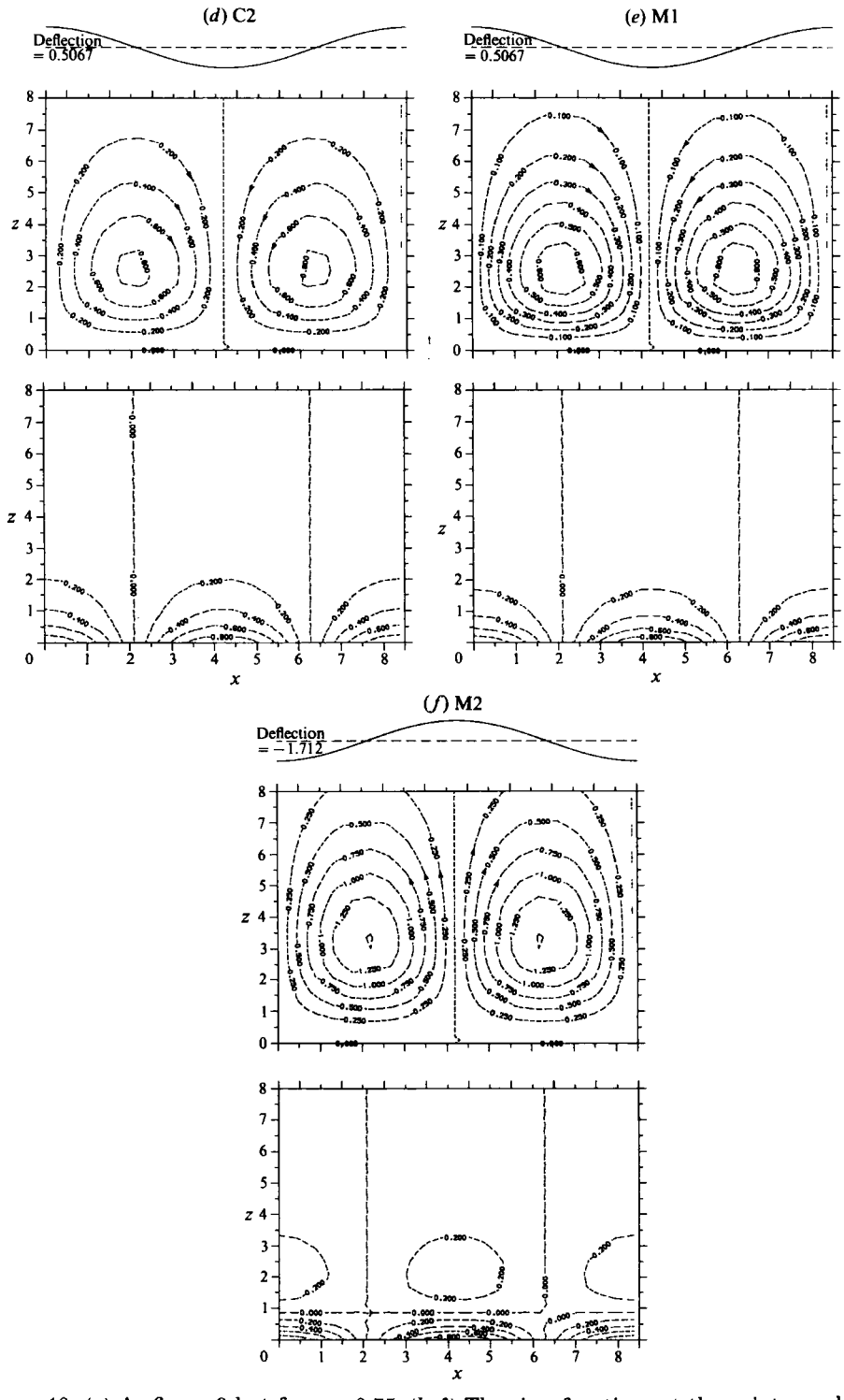

FIGURE 10. (*a*) As figure 9 but for $\alpha = 0.75$. (*b–f*) The eigenfunctions at the points marked (*b–f*) respectively in (*a*) and shows the perturbed stream function (above) and the perturbed solute concentration (below). We have normalized each eigensolution so that the perturbed concentration at (0, 0) is unity. Above each pair of contour plots is indicated the perturbed interface deflection, its phase but not its amplitude is correctly given. The maximum contour values of the perturbed stream function and solute concentration are respectively: X1, 0.8, 1; C1, 2, 1; C2, 0.8, 1; M1, 0.6, 1; M2, 1.5, 1.

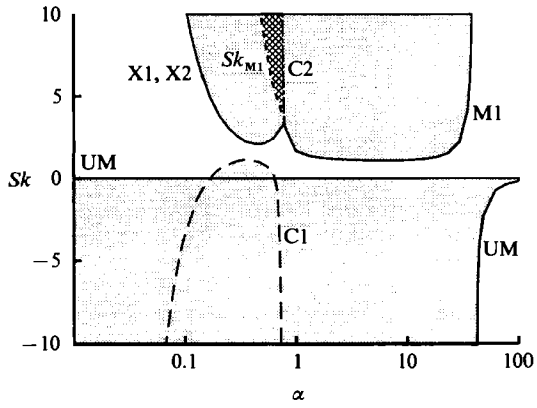

FIGURE 11. The regions of stability in (α, Sk)-space. The shaded areas represent regions in which there is at least one unstable mode and the cross-hatched area schematically represents the region in which both the M1 and C2 modes are unstable which is bounded below by the locus of the limit points Sk_{M1} which is *not* a marginal state.

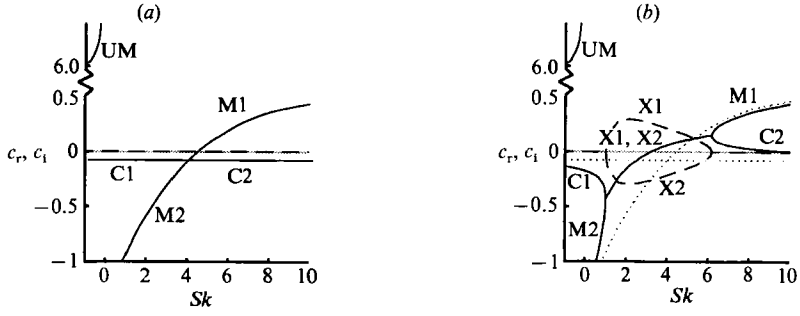

FIGURE 12. Schematic representation of the real and imaginary parts of the wave speed for (*a*) the uncoupled and (*b*) weakly coupled convective and morphological modes.

and $$F_c(\alpha, Ra) + i\alpha c = 0,$$

respectively, where F_m and F_c are complex functions of two real variables. Thus in (α, c)-space they would be represented by the curves labelled M and C as shown schematically in figure 12. The dispersion relation for the uncoupled system may be given as

$$\{F_m(\alpha, Sk) + i\alpha c\}\{F_c(\alpha, Ra) + i\alpha c\} = 0.$$

A model of the weakly coupled system is then

$$\{F_m(\alpha, Sk) + i\alpha c\}\{F_c(\alpha, Ra) + i\alpha c\} = -\epsilon g(\alpha, Sk, Ra),$$

where ϵ is a small parameter representing the magnitude of the coupling and the function g determines its precise nature.

The complex wave speed is then given by

$$c = \frac{i}{2\alpha}\{F_m(\alpha, Sk) + F_c(\alpha, Sk) \pm [(F_m(\alpha, Sk) - F_c(\alpha, Ra))^2 - 4\epsilon g(\alpha, Sk, Ra)]^{\frac{1}{2}}\}. \quad (13)$$

Away from the crossing point, where $F_m(\alpha, Sk) = F_c(\alpha, Ra)$, this may be expanded to

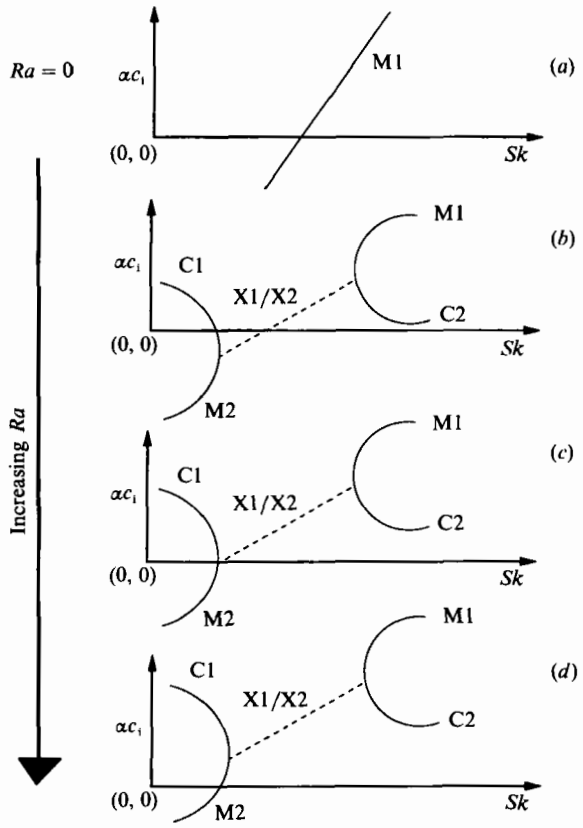

FIGURE 13. Schematic representation of the effect of increasing the Rayleigh number on the growth rate αc_i as a function of the Sekerka number. This indicates the evolution of different marginal states with increasing Rayleigh number observed in figures 2 to 7.

the following expression for the wave speeds c_c and c_m of the convective and morphological modes respectively:

$$c_m = \frac{i}{\alpha}\left[F_m(\alpha, Sk) - \frac{\epsilon g(\alpha, Sk, Ra)}{F_m(\alpha, Sk) - F_c(\alpha, Ra)} + O(\epsilon^2)\right],$$

$$c_c = \frac{i}{\alpha}\left[F_c(\alpha, Ra) - \frac{\epsilon g(\alpha, Sk, Ra)}{F_c(\alpha, Ra) - F_m(\alpha, Sk)} + O(\epsilon^2)\right] \quad \text{as} \quad \epsilon \to 0.$$

Thus, away from the crossing point the coupling acts as a regular perturbation upon the complex wave speed. However, in the vicinity of the crossing point the above expansions are singular and from (13) we find that if $g(\alpha, Sk, Ra) > 0$ then the complex wave speed remains purely imaginary, but if $g(\alpha, Sk, Ra) < 0$ the wave speed has a non-zero real part resulting in the mixed modes X1, X2, see figure 12(*b*).

Away from the crossing point where the interaction is weak we regard the coupling as perturbing the complex wave speed and so we identify a mode away from the crossing as convective or morphological depending on its proximity to the decoupled convective and morphological modes. Thus M1 and M2 are morphological modes and C1, C2 convective modes.

The above dependence of the complex wave speed upon the Sekerka number

occurs at all the non-zero values of the Rayleigh number that we have investigated. In particular the structure translates upwards in (c_i, Sk) parameter space as the Rayleigh number increases, because such an increase in the Rayleigh number destabilizes the convective modes causing the C1 and C2 modes in this space to move to larger values of c_i as Ra increases. This is the key to understanding the marginal stability curves given in figures 2–7 for different values of the Rayleigh number.

We illustrate this by considering the evolution of the modes corresponding to $\alpha = 0.5$ with increasing Rayleigh number. This is shown schematically in figure 13. At $Ra = 0$ only the morphological mode is present and there is a single non-zero value of Sk for which it is a marginal state (figures 13*a* and 2). Increasing the Rayleigh number results in the formation of the M1/C2 and C1/M2 branches at high and low values of the Sekerka number respectively which are connected by the overstable X1 and X2 modes. This provides marginal states corresponding to C1 and X1/X2 modes (figures 13*b* and 3). Increasing the Rayleigh further results in these two marginal states approaching one another and finally coalescing (figures 13*c* and 4, 5, 6). Subsequent increase in the Rayleigh number results in the birth of the single stationary M2 mode from the above coalescence (figures 13*d* and 7).

A similar argument explains the formation of the C2 marginal state at slightly higher values of the wavenumber.

In figure 10 we display plots of the eigenfunctions corresponding to different values of the Sekerka number for $\alpha = 0.5$ and $Ra = 15$ which are representative of the different modes. We note that both the morphological modes do indeed have upflow above the peaks as argued above; however, the perturbed concentration relative to the perturbed interface and flow field of the M1 and M2 modes differ by a phase of π. The convective modes C1 and C2 also show a phase change, but now in the interface deflection relative to the perturbed flow and concentration fields, which results in the two modes having different flow above the peaks. Both these phase changes are due to the M1 and C2 modes corresponding to a constitutionally supercooled situation in comparison to the M2 and C1 modes, in which this is not the case, see the end of §3.

From the above results and discussion we conclude that upflow or downflow at the cell peaks does not, in general, characterize whether a mode is morphological or convective, but is best done by determining its proximity to the uncoupled modes in (c, Sk, Ra)-space.

5.2.6. *Discussion of critical modes*

In figure 14 we plot the variation of the minimum Sekerka number of the M1 and X1, X2 modes as well as the maximum of the C1 mode with Rayleigh number. Above the curves labelled M1 and X1, X2 the system is unstable to the M1 and X1, X2 modes respectively and below the curve labelled C1 the system is unstable to the C1 mode. The shaded region indicates where the system is stable to all three modes. As this region is bounded by the M1 and C1 modes, transition to instability will only be via stationary convective or morphological modes; overstability will not be apparent at the onset of instability. This statement is true for all growth conditions of the model lead–tin alloy for which $\mathscr{U} = 6.131 \times 10^{-4}$. For lead–tin (and indeed many similar alloys) the dimensional capillarity parameter is small, which results in the dimensionless capillarity parameter $\mathscr{U}$ also being small for a wide range of growth conditions specified by the growth rate V_0 and the bulk concentration C_∞. Thus we expect the structure adumbrated above for the particular case $\mathscr{U} = 6.131 \times 10^{-4}$ to only be very weakly dependent on V_0 and C_∞ and thus representative of a wide range

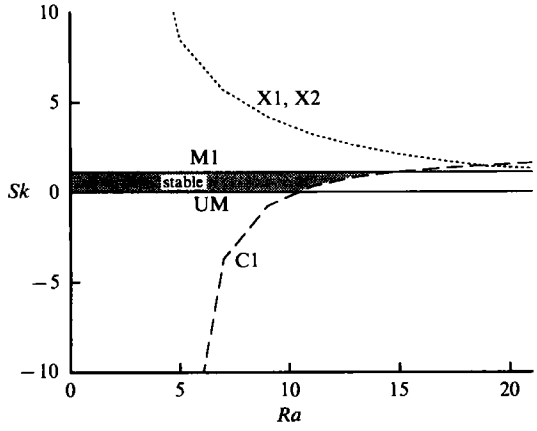

FIGURE 14. The regions of (Ra, Sk)-space in which the different modes are unstable. Above the dotted and solid curves the system is unstable to the mixed, (X1, X2) and morphological (M1) modes respectively. Below the dashed curve the system is unstable to the convective mode C1 and below the line $Sk = 0$ it is unstable to the morphological mode UM. The shaded area represents the region where it is stable to all the different modes.

of growth conditions typical of the unidirectional solidification of the lead–tin alloy, provided the dimensionless capillarity parameter is small. We note that Jenkins (1985*a*) found the transition to instability to be via the mixed modes for the situation when $\mathscr{U}$ is not small.

Coriell *et al.* (1980) also investigated this situation. They worked with dimensional quantities and found for a fixed temperature gradient of 200 K cm^{-1} that the system was unstable to a morphological mode for sufficiently large values of the growth velocity V_0 and to a convective mode for lower values. They plotted the marginal curves in (α, C_∞)-space for fixed values of V_0 and showed that the convective mode was not apparent for $V_0 \geqslant 50$ μm s^{-1}, but at $V_0 = 40$ μm s^{-1} it was present and its marginal curve was a closed loop in (α, C_∞)-space.

5.2.7. *Interpretation in dimensional parameters*

We can interpret our results in similar dimensional terms. We note from the definition of the Sekerka number and the Rayleigh number that

$$Sk/Ra = K,$$

where

$$K = -m\nu V_0^4/\mathscr{G}g\tilde{\alpha}\tilde{D}^3,$$

which is independent of the far-field concentration C_∞. Thus to compare with Coriell *et al.* (1980) we must section the marginal surfaces in (a, Sk, Ra)-space by the plane $Sk = KRa$. From figure 14 we estimate that the system will be unstable to the convective mode C1 when $K < K_{\text{crit}} \approx 0.0795$ and stable to the morphological mode M1 otherwise. Using the material and growth parameters given in table 1 we therefore deduce that the system will be convectively unstable when $V_0 \lesssim 44$ μm s^{-1}, which is in agreement with the results of Coriell *et al.* Indeed it is possible to understand all the marginal stability diagrams given by these authors for different values of V_0 by sectioning the marginal stability surfaces described above by the planes $Sk = KRa$.

We have not investigated the dependence of the marginal stability surfaces on the

Liquidus slope, m	-2.33 K wt%$^{-1}$
Solute diffusivity, $\tilde{D}$	3×10^{-5} cm^2 s^{-1}
Kinematic viscosity, ν	2.43×10^{-3} cm^2 s^{-1}
Acceleration due to gravity, g	980 cm s^{-2}
Temperature gradient, $\mathscr{G}$	200 K cm^{-1}
Coefficient of volume expansion, $\tilde{\alpha}$	5.2×10^{-3} wt%$^{-1}$

TABLE 1. Material and growth parameters for the model lead–tin alloy

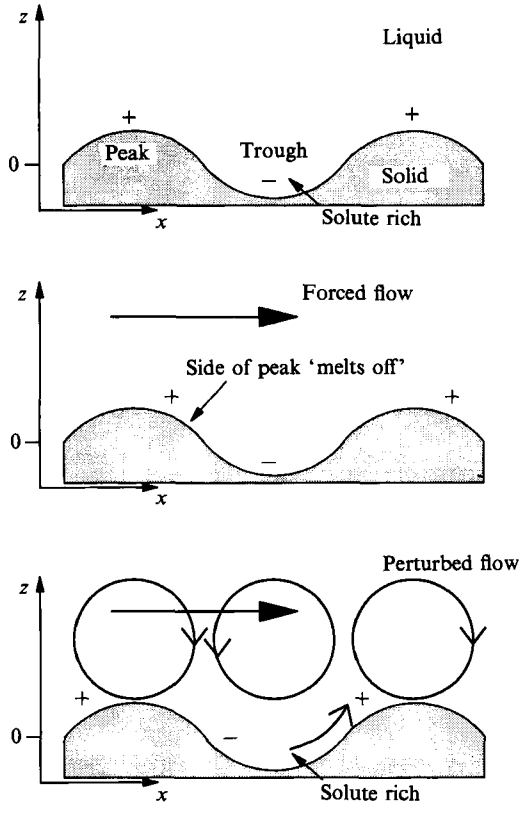

FIGURE 15. A schematic representation of the physical mechanisms involved in the formation of backward and forward travelling waves due to the presence of a shear flow. The plus and minus signs indicate the sign of the perturbed solute concentration at $z = 0$.

remaining dimensionless parameters: the segregation coefficient, k, and Schmidt number, Sc. However, inspection of the eigenvalue problem (1)–(6) indicates that

$$K_{\text{crit}} = G(k) + \mathcal{O}(Sc^{-1}) + \mathcal{O}(\mathscr{U}) \quad \text{as} \quad Sc \to \infty, \quad \mathscr{U} \to 0,$$

where $G(k)$ is an (unknown) function of a single variable. Thus for many real alloys under real growth conditions in which Sc is large and $\mathscr{U}$ is small the onset of the system to convective instability will occur when

$$V_0 < \tilde{D}(\mathscr{G}g\tilde{\alpha}/m\nu)^{\frac{1}{3}}G(k)^{\frac{1}{4}}.$$

Otherwise the onset will be via a morphological mode of instability.

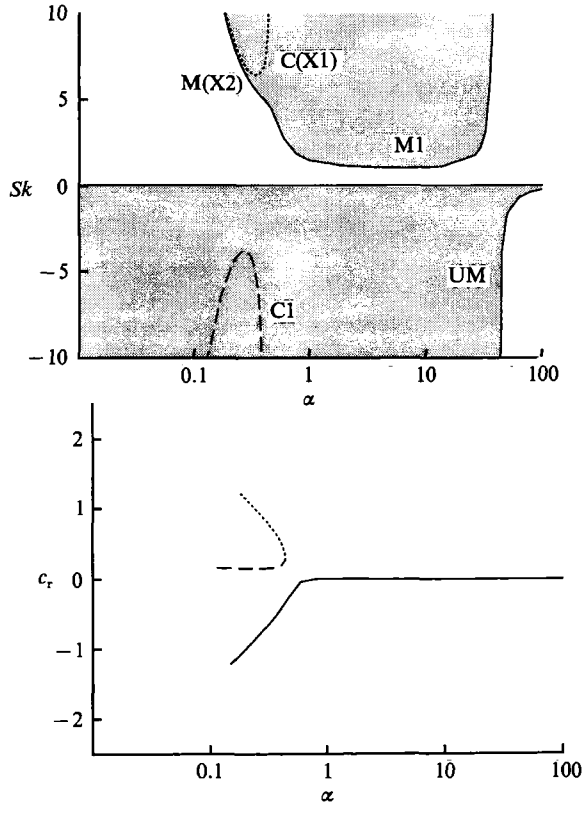

FIGURE 16. As figure 3 but for $Ra = 7$ and $Re = 5$.

6. The effect of a shear flow: $Re \neq 0$

6.1. *Shear flow alone:* $Ra = 0$

This situation was studied by Forth & Wheeler (1989) for the same model lead–tin alloy. They showed from an asymptotic analysis of the eigenvalue problem in the realistic limit $Sc \to \infty$, as well as a numerical solution, that the effect of the boundary-layer flow on the morphological mode of instability was to induce overstability by the formation of travelling waves parallel to the flow. For low wavenumber the waves travel against the direction of the flow in contrast to the high-wavenumber modes which travel in the same direction as the flow, see figure 4 of Forth & Wheeler (1989).

6.1.1. *Physical mechanisms*

Here we offer a physical explanation of this phenomena that will allow us to interpret the results presented below, when we consider the effect of both buoyancy and the boundary-layer flow. At low wavenumbers the gradually varying morphology of the interface ensures that the unperturbed boundary-layer flow is the predominant mechanism for the convective transport of solute in the perturbed system. Hence the perturbed solute is convected downstream and consequently the solute maxima of the perturbed solute are displaced downstream of the peaks of the interface. This enhances the perturbed concentration downstream of the peaks and

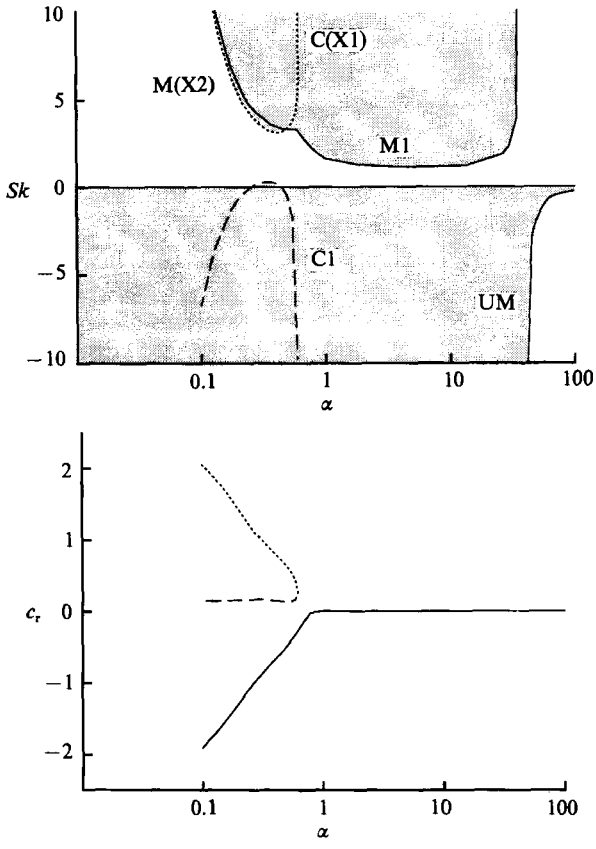

FIGURE 17. As figure 3 but for $Ra = 11$ and $Re = 5$.

so results in a local reduction of the freezing temperature which in turn causes the interface to relax back towards the colder solid phase. On the upstream side of the peaks this mechanism results in the interface advancing into the melt. The net effect is to cause the interface to propagate against the direction of the boundary-layer flow. We have confirmed this role of the unperturbed boundary-layer flow by modifying the asymptotic analysis in the limit $Sc \to \infty$ given by Forth & Wheeler (1989) to exclude the perturbed flow. This analysis shows that only waves travelling against the flow occur.

In contrast, at high wavenumbers the rapidly varying morphology of the interface ensures that both the perturbed and unperturbed flow are important in the transport of solute of the perturbed system. This results in the perturbed vertical component of the flow being approximately $\frac{1}{2}\pi$ out of phase with the perturbed solute field and interface deformation, with the perturbed concentration maxima and upflow plumes displaced to the upstream side of the peaks. This is confirmed by the asymptotic analysis of Forth & Wheeler which shows that this phase difference is $\frac{1}{2}\pi + O(Sc^{-1})$, as $Sc \to \infty$. The perturbed flow sweeps solute-rich fluid from the troughs in the direction of the flow which results in the interface relaxing behind the peaks and advancing ahead of the peaks, and consequently the formation of a travelling wave in the direction of the flow. These mechanisms are illustrated in figure 15.

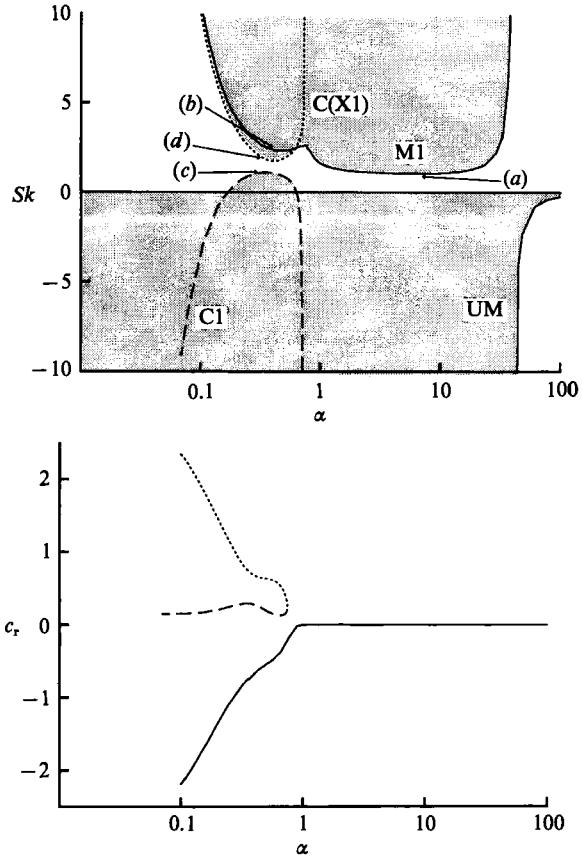

FIGURE 18. As figure 3 but for $Ra = 15$ and $Re = 5$.

6.2. *The effect of both buoyancy and shear flow: $Ra \neq 0$ and $Re \neq 0$*

In view of the large number of non-dimensional parameters in this problem we have only considered modes parallel to the flow by putting $\beta = 0$. We justify this particular choice by noting that it corresponds to the situation when the morphological modes are most affected by the presence of the boundary-layer flow, see Forth & Wheeler (1989). In order to ellucidate the situation in the presence of both flow and buoyancy effects we have repeated the computation of the eigenmodes given in §4 but for $Re = 5$. In figures 16–19 we section (α, Ra)-space for Rayleigh numbers of 7, 11, 15 and 17, with $Re = 5$.

For $Ra = 7$ we find, on comparing with the situation in the absence of flow, given in figures 3 and 16, that the marginal stability curve associated with the backward travelling mixed mode X2 is now smoothly connected onto that of the morphological mode M1. We denote the modes of the extension of the M1 mode which have negative wave speed as M(X2). In contrast, the marginal curve of the forward travelling mixed mode X1 is disconnected from the morphological mode M1 but smoothly connected to the convective mode C2; we denote this C(X1). The convective mode C1 is slightly stabilized by the presence of the flow which has transformed it into a forward travelling wave and is the least affected. Increasing the Rayleigh number results in the C(X1) and C1 modes approaching one another and finally coalescing at a Rayleigh number between 15 and 17.

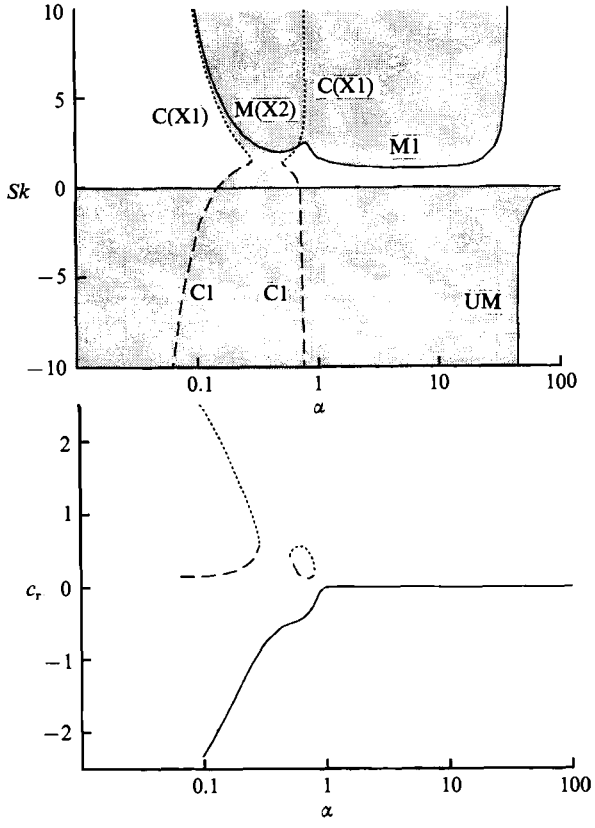

FIGURE 19. As figure 3 but for $Ra = 17$ and $Re = 5$.

6.2.1. *The shear flow as an unfolding mechanism*

The above behaviour can be understood by recognizing that the imposition of the boundary-layer flow results in a destruction of the left–right symmetry of the system which is present when $Re = 0$. It effectively unfolds the geometric structure associated with marginal curves of the non-trivial solutions of the eigenvalue problem (1)–(6). In particular, the connection between the X1, X2, M1 and M2 modes is unfolded. The smooth connection so established between the X2 and M1 mode is to be expected in the light of the formation of backward travelling waves by the morphological instability at low wavenumbers, in the presence of only a shear flow, discussed in the previous section. Indeed the variation of the wave speed along the marginal curve composed of the M1 and M(X2) modes is qualitively very similar to that predicted by the asymptotic analysis in the limit $Sc \to \infty$ given by Forth & Wheeler (1989). The physical mechanism associated with this situation given in the previous section also explains the presence of the forward travelling wave modes C(X1). If the system is not constitutionally supercooled (i.e. $Sk^{-1} - 1 + U\gamma^2 > 0$) then in the absence of a shear flow the perturbed concentration and flow fields of the C1 mode are in antiphase to the interface deflection, with upflow as well as the perturbed concentration maxima above interfacial troughs. However at the low wavenumbers associated with the C(X1) modes the predominance of the unperturbed boundary-layer flow in contributing to the perturbed lateral solute transport causes these

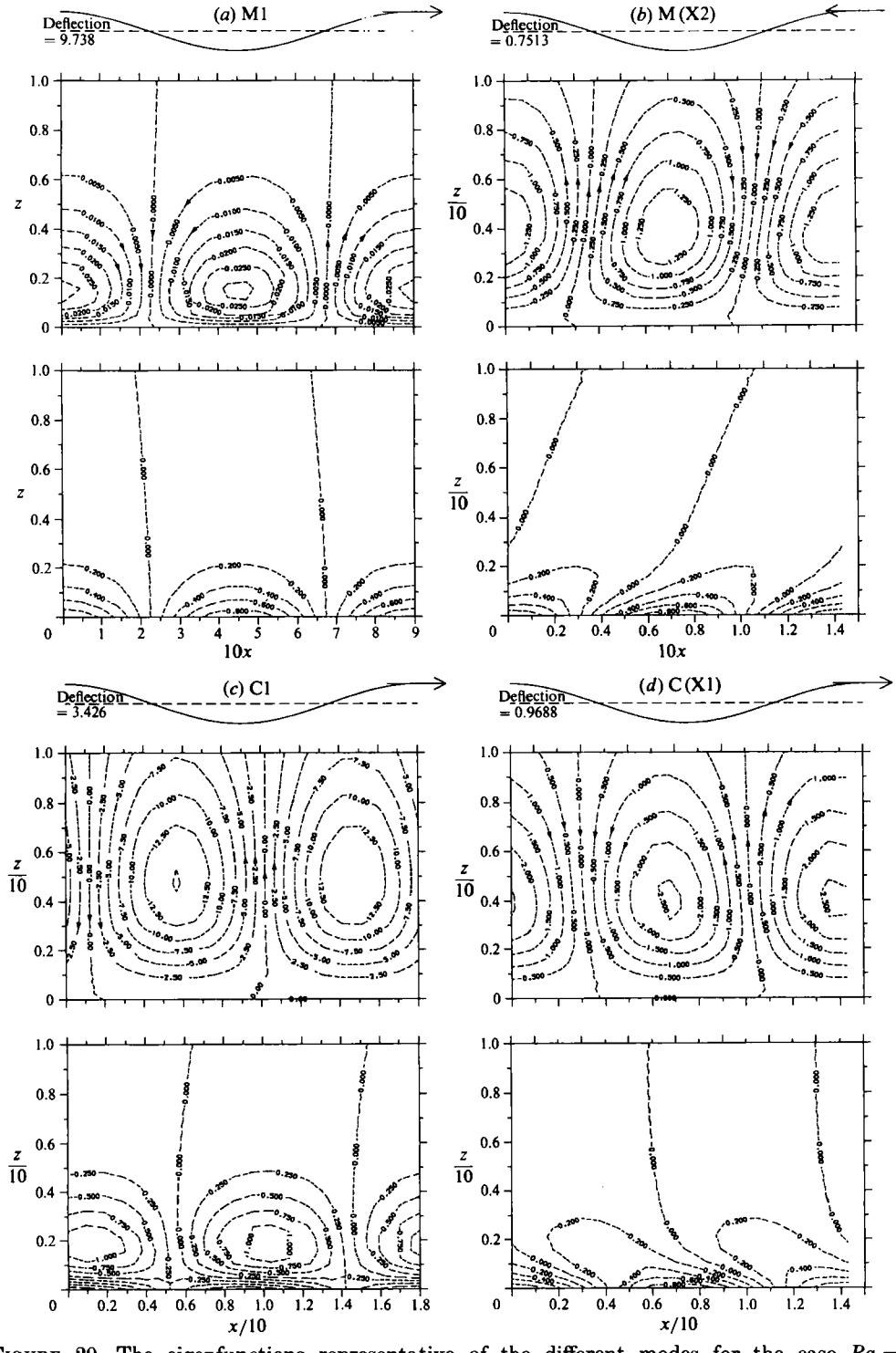

FIGURE 20. The eigenfunctions representative of the different modes for the case $Ra = 15$ and $Re = 5$. Each figure displays the eigenfunctions at the marginal states indicated by the points marked (*a–d*) in figure 18 and shows the perturbed stream function (above) and the perturbed solute concentration (below). We have normalized each eigensolution so that the perturbed concentration at (0, 0) is unity. Above each pair of contour plots is indicated the perturbed interface deflection, its phase but not its amplitude is correctly given. The maximum contour values of the perturbed stream function and solute concentration are respectively: M1, 0.03, 1; M(X2), 1.25, 1; C1, 12.5, 15; C(X1), 2.5, 1.

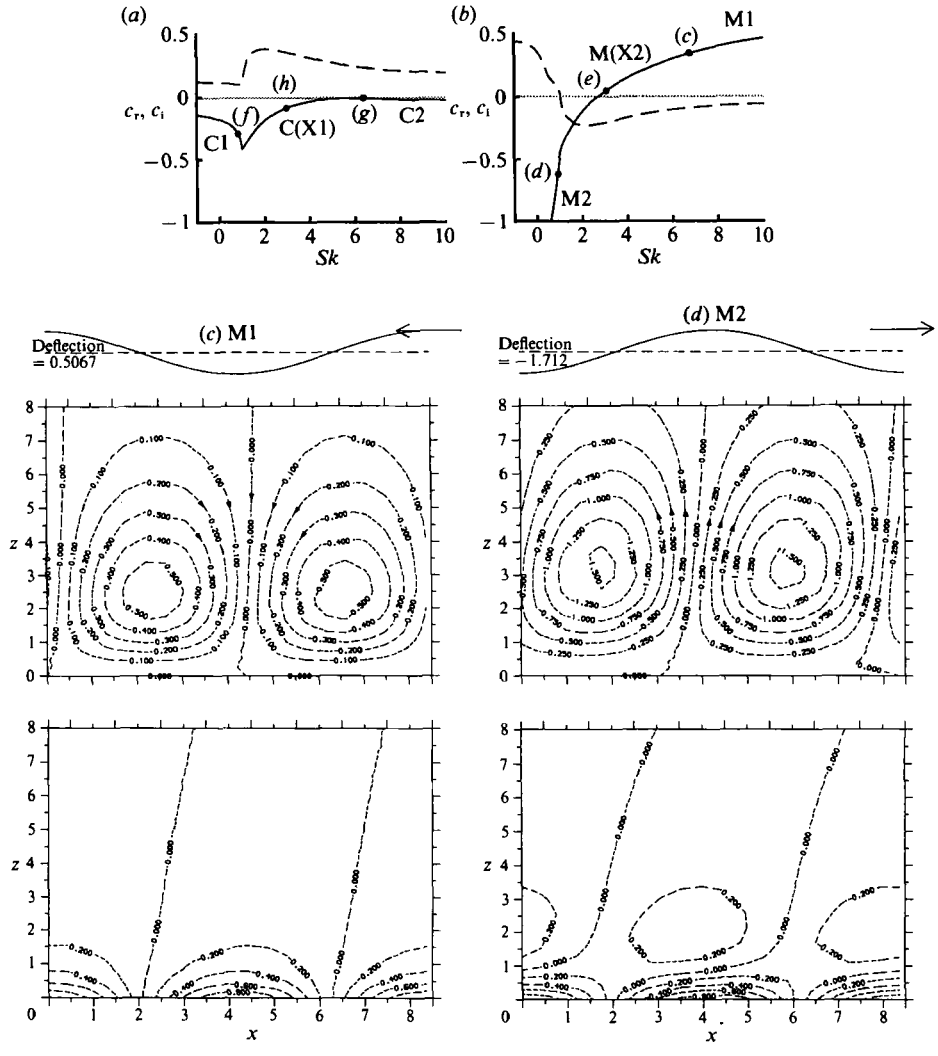

FIGURE 21 (*a–d*). For caption see facing page.

perturbed concentration maxima to be displaced upstream of the peaks and hence the formation of a forward travelling wave.

In figure 20 the eigenfunctions are presented at the stationary points of the various marginal curves for $Ra = 15$. We observe that for the M1 mode at high wavenumber the perturbed solute and flow fields are approximately $\frac{1}{2}\pi$ out of phase, in agreement with the discussion at the end of the previous section. A comparison of the M(X2) mode with its counterpart, X2, in the absence of flow shown in figure 8 shows that the perturbed flow is weakened and the interface deflection diminished by the presence of a shear flow. The convective C1 mode has been stabilized; both the stream function and the interface deflection are less that in the absence of flow, see figure 8. The C(X1) mode has a stream function qualitatively similar to the mixed mode X1, but the strength of the perturbed flow and the interface deflection are greater in the absence of an imposed flow.

That the forced flow effectively unfolds the eigenfunction solution structure is

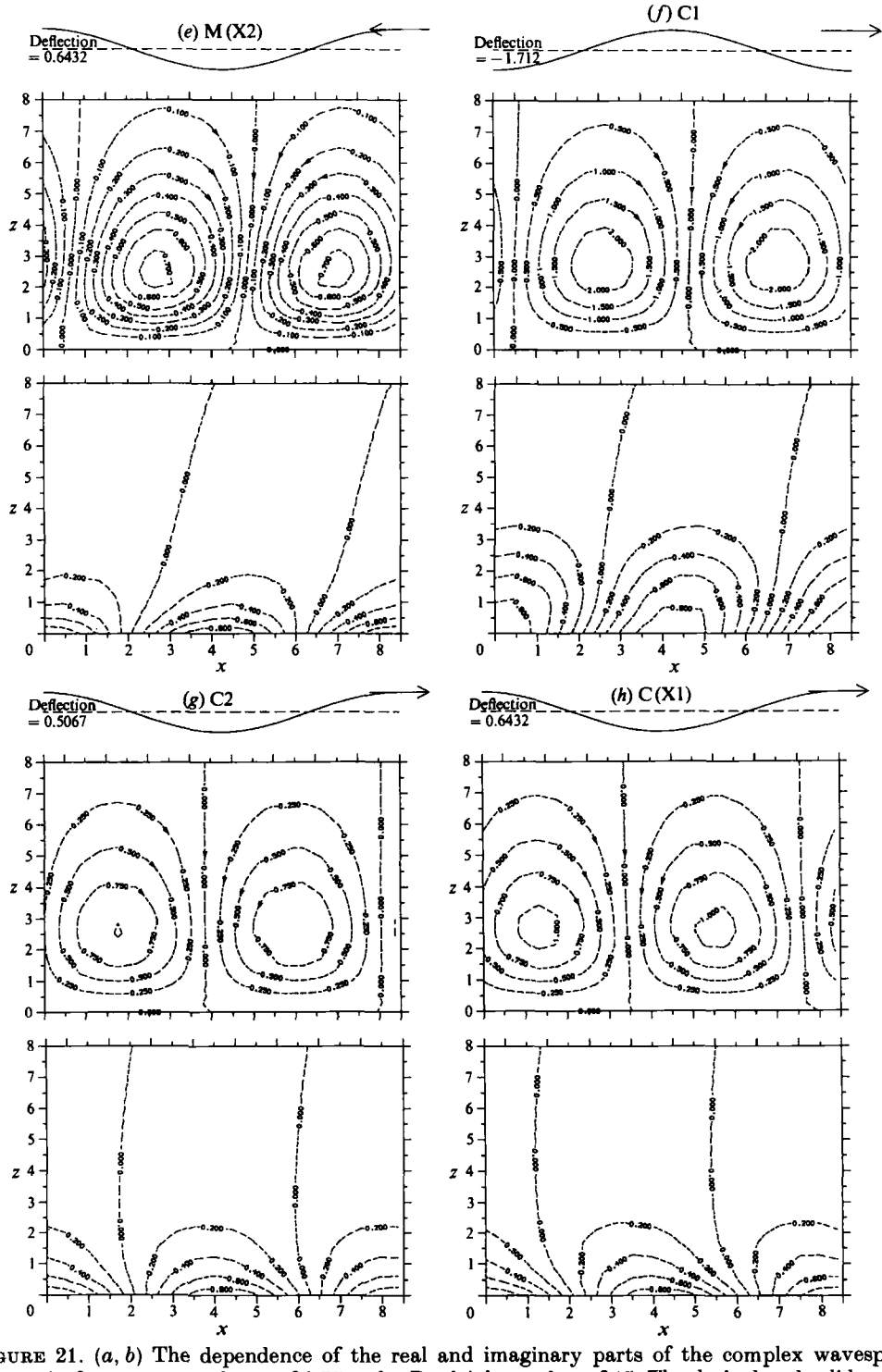

FIGURE 21. (a, b) The dependence of the real and imaginary parts of the complex wavespeed, $c = c_r + ic_i$ for a wavenumber α of 0.75 and a Rayleigh number of 15. The dashed and solid curves represent the real and imaginary parts respectively. The quantity αc_i is the growth rate of the disturbance. $(c$–$h)$ The eigenfunctions at the points marked $(c$–$h)$ respectively in figures 21(a) and 10(b) and shows the perturbed stream function (above) and the perturbed solute concentration (below). We have normalized each eigensolution so that the perturbed concentration at $(0, 0)$ is unity. Above each pair of contour plots is indicated the perturbed interface deflection, its phase but not its amplitude is correctly given. The maximum contour values of the perturbed stream function and solute concentration are respectively: M1, 0.5, 1; M2, 1.5, 1; M(X2), 0.7, 1; C1, 2, 1; C2, 1, 1; C(X2), 1, 1.

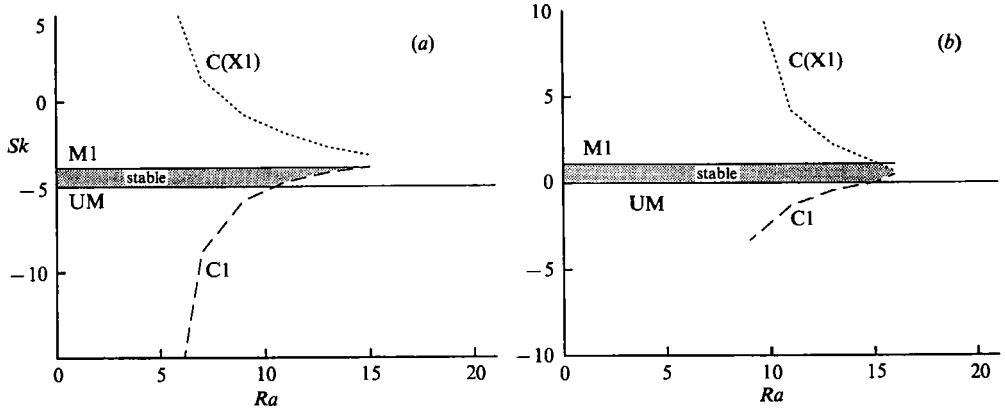

FIGURE 22. The regions of (Ra, Sk)-space in which the different modes are unstable for (*a*) $Ra = 5$, (*b*) $Ra = 50$. Above the dotted and solid curves the system is unstable to the unfolded mixed, (C(X1)) and morphological (M1) modes respectively. Below the dashed curve the system is unstable to the convective mode C1 and below the line $Sk = 0$ it is unstable to the morphological mode UM. The shaded area represents the region where it is stable to all the different modes.

further confirmed from the computation of the complex wave speed as a function of Sekerka number shown in figure 21 for $\alpha = 0.75$ when compared to their counterparts for $Re = 0$ given in figure 10(*a*). The solid lines denote c_i, where αc_i is the growth rate of the disturbance and the broken lines c_r denote the wave speed. The unfolding by the flow has transformed the X2 mode to the M(X2) mode which now smoothly connects the morphological modes M1 and M2. Further, it has also transformed the X1 into the C(X1) mode, which, in a similar way connects the C1 and C2 convective modes. This provides further evidence for our classification of the various modes as convective and morphological given above; the flow unfolds them so as to conect modes of similar nature. For this reason the flow acts to decouple the morphological and convective modes. Indeed the argument given above to model the coupling between the convective and morphological modes in the presence of buoyancy only can be extended to deal with inclusion of a shear flow. The loss of left–right symmetry can be described by requiring that the coupling function g depends on the Reynolds number, is complex and has a non-zero imaginary part when $Re \neq 0$, i.e. $g(\alpha, Sk, Ra, Re) = g_r(\alpha, Sk, Ra, Re) + iRe\, g_i(\alpha, Sk, Ra, Re)$.

6.2.2. *Discussion of critical modes*

In figure 22 we show the variation of the minimum Sekerka number of the morphological mode M1 and convective mode C(X1), as well as the maximum Sekerka number for the convective C1 for different Reynolds numbers of 5 and 50. We find that for $Re = 5$, the system (as in the case of no forced flow) is unstable to either the C1 or M1 modes, although now these modes are slowly travelling waves. In fact the wave speed of the morphological mode is insignificant, but that of the convective mode is small and positive. However, for a stronger imposed flow with $Re = 50$ the destabilization of the C(X1) mode may result in it becoming the most unstable for values of the Rayleigh number in excess of 15, in which case a forward travelling wave would be observed.

7. Conclusions

In this paper we have conducted a detailed numerical investigation of coupled convective and morphological instabilities and the effect of a shear flow upon them. We have sought to understand the complex interactions that emerge from our numerical investigation, by employing both physical and mathematical arguments.

In the absence of an imposed flow, we find that there are two morphological modes and two convective modes that are connected by two oscillatory mixed modes. We are able to confirm some of the physical mechanisms conjectured by Davis (1990) but are not able, in general, to classify a mode as convective or morphological on the basis of whether the flow above the peaks in the interface was up or down. Such a classification is too simple for this inherently complicated situation. From more mathematical arguments we conclude that this classification is best done by determining the proximity of a mode to the uncoupled modes in (c, Sk, Ra)-space.

We find for the particular case of a lead–tin alloy, at a constant temperature gradient that characterization of the *critical* mode as convective or morphological is determined solely by the ratio of the Sekerka number to the Rayleigh number. We conjecture that for a wide range of common alloys and growth conditions in which the temperature gradient is constant and the critical wavenumber and Schmidt number are large, this ratio determines the nature of the critical mode as convective or morphological and, moreover, that it depends most strongly on the segregation coefficient.

We ellucidate the physical mechanisms acting when the morphological mode is subject to an imposed flow and buoyancy is absent. From this we are able to understand how the wave speed of the neutral modes is determined in terms of the lateral transport of solute by the shear flow.

The imposed shear flow breaks the left–right symmetry and so its effect on the coupled convective and morphological modes is to unfold the complicated eigenfunction structure. This results in disconnections between the oscillatory mixed modes and the different stationary modes. This unfolding effectively uncouples the convective and morphological modes.

The authors are grateful for useful discussions with Dr S. R. Coriell, Professor S. H. Davis, Professor D. T. J. Hurle, Dr M. D. Impey, Dr G. B. McFadden and Dr D. S. Riley. S.A.F. acknowledges the receipt of a grant from the SERC.

REFERENCES

Caroli, B., Caroli, C., Misbah, C. & Roulet, B. 1985 Solutal convection and morphological instability in directional solidification of binary alloys. *J. Phys. Paris* **46**, 401–413.

Coriell, S. R., Cordes, M. R., Boettinger, W. J. & Sekerka, R. F. 1980 Convective and interfacial instabilities during unidirectional solidification of a binary alloy. *J. Cryst. Growth* **49**, 13–28.

Coriell, S. R., McFadden, G. B., Boisvert, R. F. & Sekerka, R. F. 1984 The effect of a forced Couette flow on coupled convective and morphological instabilities during directional solidification. *J. Cryst. Growth* **69**, 15–22.

Coriell, S. R., McFadden, G. B. & Sekerka, R. F. 1985 Cellular growth during directional solidification. *Ann. Rev. Mater. Sci.* **15**, 119–145.

Coriell, S. R., McFadden, G. B., Voorhees, P. W. & Sekerka, R. F. 1987 Stability of a planar interface during solidification of a multicomponent system. *J. Cryst. Growth* **82**, 295–302.

Davis, S. H. 1990 Hydrodynamic interactions in directional solidification. *J. Fluid Mech.* **212**, 241–262.

Delves, R. T. 1968 Theory of the stability of a solid–liquid interface during growth from sitrred melts. *J. Cryst. Growth* **3, 4**, 562–568.

Delves, R. T. 1971 Theory of stability of a solid–liquid interface during growth from stirred melts. II. *J. Cryst. Growth* **8**, 13–25.

Forth, S. A. 1989 Morphological and hydrodynamic instabilities in unidirectional alloy solidification. Ph.D. thesis, University of Bristol, England.

Forth, S. A. & Wheeler, A. A. 1989 Hydrodynamic and morphological stability of the unidirectional solidification of a freezing binary alloy: a simple model. *J. Fluid Mech.* **202**, 339–366.

Gershuni, G. Z. & Zhukhovitskii 1976 *Convective Stability In Incompressible Fluids*. Jerusalem: Keter.

Glicksman, M. E., Coriell, S. R. & McFadden, G. B. 1986 Interaction of flows with the crystal–melt interface. *Ann. Rev. Fluid Mech.* **18**, 307–35.

Hurle, D. T. J., Jakeman, E. & Wheeler, A. A. 1982 Effect of solutal convection on the morphological stability of a binary alloy. *J. Cryst. Growth* **58**, 163–179.

Hurle, D. T. J., Jakeman, E. & Wheeler, A. A. 1983 Hydrodynamic stability of the melt during solidification of a binary alloy. *Phys. Fluids* **26**, 624–626.

Jenkins, D. R. 1985*a* Nonlinear analysis of convective and morphological instability during solidification of a dilute binary alloy. *Physicochem. Hydrodyn.* **6**, 521–537.

Jenkins, D. R. 1985*b* Nonlinear interaction of morphological and convective instabilities during solidification of a dilute binary alloy. *IMAJ Appl. Maths* **35**, 145–157.

Jenkins, D. R. 1990 Oscillatory instability in a model of directional solidification. *J. Cryst. Growth* **102**, 481–490.

Keller, H. B. 1976 *Numerical Solution of Two Point Boundary Value Problems*. SIAM.

Langer, J. S. 1980 Instabilities and pattern formation in crystal growth. *Rev. Mod. Phys.* **52**, 1–28.

McFadden, G. B., Coriell, S. R. & Alexander, J. I. D. 1988 Hydrodynamic and free boundary instabilities during crystal growth: the effect of a plane stagnation flow. *Comm. Pure Appl. Maths* **41**, 683–706.

Mullins, W. W. & Sekerka, R. F. 1964 Stability of a planar interface during solidification of a dilute binary alloy. *J. Appl. Phys.* **35**, 444–451.

Ng, B. S. & Reid, W. H. 1980 On the numerical solution of the Orr–Somerfeld problem: asymptotic initial conditions for shooting methods. *J. Comput. Phys.* **38**, 275–293.

Riley, D. S. & Davis, S. H. 1990 Long-wave interactions in morphological and convective instabilities. *SIAM J. Appl. Maths* **50**, 420–436.

Rutter, J. W. & Chalmers, B. A. 1953 A prismatic substructure formed during solidification of metals. *Can. J. Phys.* **31**, 15–39.

Schaeffer, R. J. & Coriell, S. R. 1982 Convective and interfacial instabilities during solidification of succinonitrile containing ethanol. In *Materials Processing in the Reduced Gravity Environment of Space*. (ed. G. E. Rindone), pp. 479–489. Elsevier.

Scott, M. R. & Watts, H. A. 1975 SUPORT: A computer code for two point boundary values problems via orthonormalisation. *SAND* 75-0198. Albuquerque: Sandia Laboratories.

Ungar, L. H. & Brown, R. A. 1984 Cellular interface morphologies in directional solidification. The one-sided model. *Phys. Rev.* B **29**, 1367–1380.

Wollkind, D. J. & Segel, L. A. 1970 A nonlinear stability analysis of the freezing of a dilute binary alloy. *Phil. Trans. R. Soc. Lond.* A **268**, 351–380.